

Gravitational wave emission and spindown of young pulsars

Mark G. Alford and Kai Schwenzer

Department of Physics, Washington University, St. Louis, Missouri, 63130, USA

The rotation frequencies of young pulsars are systematically below their theoretical Kepler limit. R-modes have been suggested as a possible explanation for this observation. With the help of semi-analytic expressions that make it possible to assess the uncertainties of the r-mode scenario due to the impact of uncertainties in underlying microphysics, we perform a quantitative analysis of the spin-down and the emitted gravitational waves of young pulsars. We find that the frequency to which r-modes spin down a young neutron star is surprisingly insensitive both to the microscopic details and the saturation amplitude. Comparing our result to astrophysical data, we show that for a range of sufficiently large saturation amplitudes r-modes provide a viable spindown scenario and that all observed young pulsars are very likely already outside the r-mode instability region. Therefore the most promising sources for gravitational wave detection are unobserved neutron stars associated with recent supernovae, and we find that advanced LIGO should be able to see several of them. We find the remarkable result that the gravitational wave strain amplitude is completely independent of both the r-mode saturation amplitude and the microphysics, and depends on the saturation mechanism only within some tens of per cent. However, the gravitational wave frequency depends on the amplitude and we provide the required expected timing parameter ranges to look for promising sources in future searches.

I. INTRODUCTION

A neutron star is a complex system whose behavior is influenced by physics on scales from the Fermi scale to its size and whose description involves all forces of nature. This holds in particular when dynamical aspects involving mechanical oscillations coupled to radiation fields are considered and a description should thereby intricately depend on all these details. Yet, the surprising finding presented in this work is that for the relevant observables analytic expressions can be derived that are strikingly insensitive to these complicated microscopic as well as macroscopic details.

The rotation frequencies of pulsars, as well as their time derivatives, are among the most precise observations in physics. These frequencies change over time due to magnetic braking and other possible spindown mechanisms like gravitational wave emission due to deformations or oscillation modes of the star. In particular the unstable r-modes [1, 2] are interesting because they must be stabilized by a viscous dissipation mechanism and thereby can probe the microphysics deep inside the star. It has already been shown [3, 4] that important static aspects of the instability regions of r-modes are very insensitive to quantitative microscopic details but do depend on qualitative differences of the various possible forms of dense matter. Here we extend this study to the dynamical r-mode evolution of neutron stars and show that in this case the insensitivity to unknown input parameters is even more pronounced. In particular we derive semi-analytic expressions for the final frequency of the spindown evolution and the spindown time of young neutron stars [5] and show that these quantities are likewise insensitive to the particular r-mode saturation mechanism.

Magnetic dipole radiation is considered as a standard mechanism for the spindown of pulsars and is used to determine an approximate characteristic spindown age

[6]. In contrast, in this work we will instead only consider the spindown torque due to r-modes, which is only non-vanishing as long as the star is within the unstable region. Our results therefore provide upper limits on the actual frequencies of observed pulsars and should apply as long as the r-mode spindown dominates. However, they might not be applicable to magnetars where this is not guaranteed. A more detailed analysis which includes both electromagnetic and gravitational radiation [7, 8] and thereby allows to make contact to pulsar ages will be given elsewhere.

The fastest young pulsar observed so far is PSR J0537-6910 with a rotational frequency of $f \approx 62$ Hz, which has been associated to the remnant N157B of a supernova that exploded in the Large Magellanic Cloud [9]. We find that this spin frequency is just below the final frequency due to pure r-mode emission of a neutron star with standard modified Urca beta equilibration processes, so that r-mode emission could indeed provide a quantitative explanation for the low spin frequencies of young neutron stars. If the r-mode scenario is realized, the fact that all observed stars are below the r-mode bound also suggests that r-mode spindown should be fast, i.e. at least comparable to magnetic spindown, which would require a high r-mode saturation amplitude $\alpha \gtrsim 0.01$ in young neutron stars.

For standard damping, i.e. in the absence of hypothetical strong additional sources of dissipation, r-modes of neutron stars are an important source of gravitational waves and provide an interesting possibility for their detection since r-modes can radiate over long times. Our results on the spindown show that if r-modes explain young neutron star spins, that implies a large saturation amplitude which in turn says that the window of opportunity for direct observation is brief. Promising sources are therefore very young and so far undetected rapidly spinning neutron stars. Previously analytic esti-

mates have been given for the gravitational wave strain of r-modes of young stars [10]. However, this work did not take into account the limited observation time in practical gravitational wave searches and found unrealistically large signal-to-noise ratios. Using the semi-analytic expression for the r-mode evolution we perform a comprehensive analysis of the gravitational wave emission. We find the remarkable result that the gravitational wave emission from r-modes in young pulsars is *independent* of the saturation amplitude and even shows hardly any dependence on the saturation mechanism. This allows us to give surprisingly definite predictions for the gravitational wave signal despite our limited understanding of these complicated systems. We compare our results to the detector sensitivities for realistic searches that take into account our ignorance of the detailed properties of the source and find that forthcoming second generation detectors like advanced LIGO [11, 12] are sensitive enough to see several potential sources.

II. MATERIAL AND STAR PROPERTIES

As noted before a neutron star is a complex system and the description of its spindown evolution requires an understanding of various different aspects. The starting point is the static star configuration which is determined by gravity as described by the general relativistic Oppenheimer-Volkoff (OV) equations [13, 14]. The latter require the equation of state of charge-neutral dense matter in beta equilibrium as an ingredient which is determined by microscopic strong interactions. Both the rotation and the oscillation of the star are modeled as perturbations of the static respectively the rotating star configuration [15]. For simplicity both are standardly obtained from the Newtonian ¹ Euler-equation of a non-viscous fluid. The classical r-modes with $l = m$ are given by the Eulerian velocity perturbations

$$\delta\vec{v} = \alpha R\Omega \left(\frac{r}{R}\right)^m \vec{Y}_{mm}^B(\theta, \varphi) e^{i\omega t}, \quad (1)$$

where α is a dimensionless amplitude parameter, R is the star radius, Ω and ω are rotational and mode angular velocity, respectively, and \vec{Y}^B is the magnetic vector spherical harmonic with magnetic quantum number m .

To describe the dynamical evolution requires microscopic material properties of the dense matter within the

star. Here we follow the method that was developed previously in [3] and [4] to obtain semi-analytic results for the boundary of the r-mode instability region as well as for the saturation amplitude in case suprathreshold bulk viscosity saturates the mode. The basic idea is that the microscopic material properties that are relevant for the pulsar evolution have - at least over the range required to describe the relevant aspects - simple power law dependencies on the temperature T , the oscillation frequency ω and the density oscillation amplitude $\Delta n/\bar{n}$. The required quantities for the star evolution are the shear viscosity η , the bulk viscosity ζ , the specific heat c_V and the neutrino emissivity ϵ . Both the bulk viscosity and the neutrino emissivity are determined by a weak equilibration process whose rate in a degenerate system has the form $\Gamma^{(\leftrightarrow)} = -\tilde{\Gamma}T^\delta\mu_\Delta$, where μ_Δ is the chemical potential difference that is driven out of equilibrium. As discussed below, for our present analysis the suprathreshold amplitude dependence of the bulk viscosity and the neutrino emissivity [16, 17] does not have a significant impact and we will discuss their impact in other situations in more detail in a future work. In the subthermal regime these quantities can generally be parameterized as

$$\eta = \tilde{\eta}T^{-\sigma}, \quad \zeta \approx \frac{C^2\tilde{\Gamma}T^\delta}{\omega^2 + (B\tilde{\Gamma}T^\delta)^2} \rightarrow \frac{C^2\tilde{\Gamma}T^\delta}{\omega^2}, \quad (2)$$

$$c_V = \tilde{c}_VT^v, \quad \epsilon \approx \tilde{\epsilon}T^\theta, \quad (3)$$

where B and C are non-equilibrium susceptibilities. With such power law behavior it is clear that physical results should depend far more sensitively on the exponents σ , δ , v and θ than on the prefactor functions $\tilde{\eta}$, \tilde{c}_V , $\tilde{\epsilon}$, \dots . The important point is that the exponents are the same for a given phase of dense matter, like e.g. hadronic matter with modified Urca reactions [18], and quantitative details due to the unknown equation of state or the interactions are only reflected in the prefactors. Strikingly we will see below that the quantitative dependence on these prefactors can be even far more insensitive than this general argument suggests. Different phases of dense matter, however, can feature qualitatively different low energy degrees of freedom resulting in different exponents and thereby can lead to a qualitatively very different star evolution.

The above material properties are local quantities, but all that enters the evolution equations below are quantities that are averaged over the entire star. These are the power radiated in gravitational waves P_G , the dissipated power P_S and P_B due to shear and bulk viscosity, the specific heat of the star C_V , the total neutrino luminosity L_ν and the moment of inertia I [3, 10]

¹ This Newtonian approximation, as well as the approximation to use the Eulerian density fluctuation instead of the Lagrangian fluctuation to evaluate eq. (12) below (see [15] for details), is only used for numerical estimates. The general semi-analytic expressions derived in this work are - with appropriate parameter values - valid in the fully relativistic case and do not rely on such approximations. These results will show that the impact of these approximations on the final observables is small.

parameter of the ...	integral expression
moment of inertia	$\tilde{I} \equiv \frac{8\pi}{3MR^2} \int_0^R dr r^4 \rho$
radiated power	$\tilde{J}_m \equiv \frac{1}{MR^{2m}} \int_0^R dr r^{2m+2} \rho$
shear dissipated power	$\tilde{S}_m \equiv \frac{1}{R^{2m+1} \Lambda_{\text{QCD}}^{3+\sigma}} \int_{R_i}^{R_o} dr r^{2m} \tilde{\eta}$
bulk dissipated power	$\tilde{V}_m \equiv \frac{\Lambda_{\text{EW}}^4}{R^3 \Lambda_{\text{QCD}}^{9-\delta}} \int_{R_i}^{R_o} dr r^2 A^2 C^2 \tilde{\Gamma} (\delta \Sigma_m)^2$
specific heat	$\tilde{C}_V \equiv \frac{1}{R^3 \Lambda_{\text{QCD}}^{3-v}} \int_{R_i}^{R_o} dr r^2 \tilde{c}_V$
neutrino luminosity	$\tilde{L} \equiv \frac{\Lambda_{\text{EW}}^4}{R^3 \Lambda_{\text{QCD}}^{9-\theta}} \int_{R_i}^{R_o} dr r^2 \tilde{\epsilon}$

Table I: Radial integral parameters encoding the complete information on the star's interior - i.e. on the microphysical transport properties, the equation of state and the star's density profile.

$$P_G = \frac{32\pi (m-1)^{2m} (m+2)^{2m+2}}{((2m+1)!!)^2 (m+1)^{2m+2}} \tilde{J}_m^2 G M^2 R^{2m+2} \alpha^2 \Omega^{2m+4}, \quad (4)$$

$$P_S = -\frac{(m-1)(2m+1) \tilde{S}_m \Lambda_{\text{QCD}}^{3+\sigma} R^3 \alpha^2 \Omega^2}{T^\sigma}, \quad (5)$$

$$P_B = -\frac{16m}{(2m+3)(m+1)^5 \kappa^2} \frac{\tilde{V}_m \Lambda_{\text{QCD}}^{9-\delta} R^7 \alpha^2 \Omega^4 T^\delta}{\Lambda_{\text{EW}}^4}, \quad (6)$$

$$C_V = 4\pi \Lambda_{\text{QCD}}^{3-v} R^3 \tilde{C}_V T^v, \quad (7)$$

$$L_\nu = \frac{4\pi R^3 \Lambda_{\text{QCD}}^{9-\theta} \tilde{L}}{\Lambda_{\text{EW}}^4} T^\theta, \quad (8)$$

$$I = \tilde{I} M R^2. \quad (9)$$

where Λ_{QCD} and Λ_{EW} are characteristic strong and electroweak scales introduced to make these quantities dimensionless. With the energy of the r-mode

$$E_m = \frac{1}{2} \alpha^2 \Omega^2 M R^2 \tilde{J} \quad (10)$$

one can define characteristic time scales for the r-mode growth τ_G and the viscous damping τ_S and τ_B via

$$\frac{1}{\tau_i} = -\frac{P_i}{2E_m}. \quad (11)$$

so τ_G is negative and τ_S and τ_B are positive. The above quantities are given in terms of parameters that involve the integration over the star or alternatively over the layer(s) ranging from R_i to R_o that contribute(s) dominantly to this quantity. These are defined in table I.

All quantities appearing in these integrals, like the energy density ρ , the inverse squared speed of sound A , the non-equilibrium susceptibility C and the r-mode density oscillation

$$\delta \Sigma \equiv \frac{m+1}{2\alpha A R^2 \Omega^3} \sqrt{\frac{(m+1)^3 (2m+3)}{4m}} \left(\int d\Omega \left| \vec{\nabla} \cdot \delta \vec{v} \right|^2 \right)^{\frac{1}{2}} \quad (12)$$

depend on the position within the star via their density dependence. These few constants encode the complete information on the physics inside the star and are sufficient to calculate the star evolution.

The dimensionless parameters \tilde{I} and \tilde{J} , arising in the moment of inertia and the canonical energy and angular momentum of the mode, involve integrals over the energy density in which the outer parts are strongly weighted by high powers of r . They are normalized by the mass and appropriate powers of the radius so that the range these constants can vary over is independent of the mass. The mass by which these constants are divided is given by an analogous integral with a smaller power of r . Consequently these constants are large for stars whose mass is strongly spread out but small for stars where the mass is concentrated close to the center. Since the energy density is a monotonically decreasing function, it is clear that \tilde{I} and \tilde{J} are bounded from above by the values for a constant density star [3]. Similarly, lower bounds can be obtained by noting that in a star the mass cannot be arbitrarily concentrated. A limit for the energy density at a given radius is obtained by the constraint that the matter within this radius has to be stable against gravitational collapse. The corresponding bound for the energy density is given by $\rho(r) < 1/(8\pi G r^2)$ which can be integrated to obtain lower bounds on \tilde{I} and \tilde{J} . Combining these rigorous limits we find that for any compact star these parameters are narrowly bounded within roughly a factor of two

$$0.22 \approx \frac{2}{9} \leq \tilde{I} \leq \frac{2}{5} = 0.4, \quad (13)$$

$$1.59 \cdot 10^{-2} \approx \frac{1}{20\pi} \leq \tilde{J} \leq \frac{3}{28\pi} \approx 3.41 \cdot 10^{-2}. \quad (14)$$

However, for a neutron star with a crust the energy density vanishes at the surface and therefore the upper bounds should even clearly overestimate the realistic range. Assuming expected mass and radius ranges of a neutron star $1 M_\odot \lesssim M \lesssim 2.5 M_\odot$ and $10 \text{ km} \lesssim R \lesssim 15 \text{ km}$, the moment of inertia eq. (9) is therefore uncertain within at most an order of magnitude

$$4.4 \times 10^{44} \frac{\text{g}}{\text{cm}^2} \lesssim I \lesssim 4.5 \times 10^{45} \frac{\text{g}}{\text{cm}^2}. \quad (15)$$

The uncertainty on the other parameters arises both from the microscopic quantities eqs. (2) and (3) as well as from the particular (baryon) density profile $n(r)$ which in turn depends both on the equation of state and the particular solution of the OV equations (parameterized e.g. by the star's mass). All parameters defined above in tab. I are given for different stars in tab. II. For illustration of our semi-analytic results below we consider different stars with an APR equation of state [19]. In these stars we assume that the core of the star dominates the relevant quantities and neglect possible contributions from the crust. For the maximum mass APR star the density

is high enough that direct Urca processes are kinematically allowed within an inner core².

III. PULSAR EVOLUTION EQUATIONS

The evolution equations are obtained from energy and angular momentum conservation laws [10, 20, 21] and take the form

$$\frac{d\alpha}{dt} = -\alpha \left(\frac{1}{\tau_G} + \frac{1}{\tau_V} \left(\frac{1 - Q\alpha^2}{1 + Q\alpha^2} \right) \right), \quad (16)$$

$$\frac{d\Omega}{dt} = -\frac{2\Omega Q\alpha^2}{\tau_V} \frac{1}{1 + Q\alpha^2}, \quad (17)$$

$$\frac{dT}{dt} = -\frac{1}{C_V} (L_\nu - P_V), \quad (18)$$

with $Q \equiv 3\tilde{J}/(2\tilde{I})$ and in terms of the viscous dissipated power $P_V = P_S + P_B + \dots$ and damping time $1/\tau_V \equiv 1/\tau_S + 1/\tau_B + \dots$, where the dots denote possible other dissipative mechanisms, like boundary layer effects. Here we include the reheating due to the dissipated power P_V within the star, that was partly neglected in [10]. Using the previous bounds on the parameters \tilde{I} and \tilde{J} we see that $Q < 81/(112\pi) \approx 0.23$ so that the factors $1 \pm Q\alpha^2$ are only relevant for large amplitude modes with $\alpha \gtrsim 1$, i.e. in a regime where the perturbative approximation for the r-mode [15] breaks down anyway. The r-mode is unstable when the right hand side of the amplitude equation eq. (16) is positive, i.e. when $\tau_V|_{\alpha=0} \geq -\tau_G$, where the equality defines the boundary of the instability region [3]. Since the r-mode will grow once it enters the instability region the evolution requires a non-linear mechanism to saturate the amplitude at a finite value. A simple possibility is the suprathreshold enhancement of the bulk viscosity [4, 16, 22]. Unfortunately when only the damping in the core is considered, this mechanism saturates the mode only at rather large amplitudes. The bulk viscosity contribution of the inner crust might change this since the outer regions of the star are strongly weighted by the suprathreshold viscosity [4], but the bulk viscosity has not been computed at this point. Another promising mechanism is the non-linear coupling of the r-mode to other daughter modes that are subsequently damped by viscosity [23–25]. Further possibilities include non-linear hydrodynamic effects [26, 27] or turbulent crust-core boundary layer damping [28] but at this point it is not settled which of these mechanisms will actually saturate the mode³. Therefore, we follow

here the approach pursued in [10] and will not study a particular saturation mechanism but simply assume that a corresponding mechanism operates and saturates the r-mode at a particular amplitude α_{sat} . In contrast to the above explicit mechanisms, α_{sat} is in this case an unknown parameter that may depend on Ω or T and we will study the dependence of our results on it below.

At saturation $d\alpha/dt = 0$, so from eq. (16),

$$\frac{1}{\tau_V} = \frac{1}{\tau_G} \left(\frac{1 + Q\alpha^2}{1 - Q\alpha^2} \right) \xrightarrow{\alpha \ll 1/\sqrt{Q}} \frac{1}{\tau_G}, \quad (19)$$

and likewise $P_V \rightarrow P_G$. This simply says that at saturation there must be a sufficiently strong source of dissipation to overcome the gravitational instability. Making the replacements in eqs. (16), (17) and (18) leaves the reduced set

$$\frac{d\Omega}{dt} = -\frac{2\Omega}{|\tau_G|} \frac{Q\alpha_{\text{sat}}^2}{1 - Q\alpha_{\text{sat}}^2} \approx -\frac{2Q\alpha_{\text{sat}}^2\Omega}{|\tau_G|}, \quad (20)$$

$$\frac{dT}{dt} = -\frac{1}{C_V} \left(L_\nu + P_G \left(\frac{1 + Q\alpha_{\text{sat}}^2}{1 - Q\alpha_{\text{sat}}^2} \right) \right) \approx -\frac{1}{C_V} (L_\nu + P_G), \quad (21)$$

where, as argued before, the approximate expressions hold over nearly the entire range of physically reasonable amplitudes. Note that compared to [10] we take into account that according to eq. (19) the saturation mechanism dissipates a significant amount of energy that heats the star. The only way that this could be avoided is if some of the corresponding energy is directly, non-thermally radiated away, e.g. in neutrinos or electromagnetic radiation. In all proposed mechanisms, like the non-linear enhancement of the bulk viscosity [4, 22], mode-coupling to viscously damped daughter modes [23, 24] or nonlinear hydrodynamic effects [26, 27], such a radiative component is negligible and nearly all the dissipated energy eventually ends up as heat. Photons are only emitted from the surface and the emission process is not affected in any significant way by oscillation modes. For neutrinos the additional emission due to a global mode is described by the amplitude-dependent, suprathreshold regime of the neutrino emissivity [17, 29]. The neutrino luminosity of a neutron star is compared to the viscously dissipated power in fig. 1. As can be seen the suprathreshold neutrino luminosity, characterized by the steeply rising part, becomes relevant compared to the shear viscosity only at amplitudes $\alpha = O(1)$; whereas at lower amplitudes the energy loss by non-thermal, induced neutrino emission is entirely negligible. Daughter modes arising in mode-coupling mechanisms have lower amplitudes and

² The density becomes large enough at the center so that the direct Urca channel opens for stars with masses slightly above $2M_\odot$.

³ A reason for this is that because of the complexity of the system all of these analyses have to make simplifications. For instance in mode coupling scenarios the possible interactions have to be

restricted in the analysis, whereas in hydrodynamical simulations the radiation reaction force needs to be artificially increased to make the computation numerically feasible, see also [23].

neutron star	shell	$R [km]$	$\Omega_K [Hz]$	\tilde{I}	\tilde{J}	Q	\tilde{S}	\tilde{V}	\tilde{C}_V	\tilde{L}	σ	δ	v	θ
APR $1.4 M_\odot$	core	11.5	6020	0.283	1.81×10^{-2}	0.096	7.68×10^{-5}	1.31×10^{-3}	2.36×10^{-2}	1.91×10^{-2}	$\frac{5}{3}$	6	1	8
APR $2.0 M_\odot$		11.0	7670	0.300	2.05×10^{-2}	0.102	2.25×10^{-4}	1.16×10^{-3}	2.64×10^{-2}	1.69×10^{-2}				
APR $2.21 M_\odot$	m.U. core	10.0	9310	0.295	2.02×10^{-2}	0.103	5.05×10^{-4}	9.34×10^{-4}	2.62×10^{-2}	1.29×10^{-2}	$\frac{5}{3}$	4	1	6
	d.U. core							1.16×10^{-8}		$2.31 \cdot 10^{-5}$				

Table II: Parameters characterizing the neutron star considered in this work. The constants \tilde{I} , \tilde{J} , \tilde{S} , \tilde{V} , \tilde{C}_V and \tilde{L} are given in tab. I using the generic normalization scales $\Lambda_{\text{QCD}} = 1 \text{ GeV}$ and $\Lambda_{\text{EW}} = 100 \text{ GeV}$ and the temperature exponents σ , δ , v and θ are defined by eqs. (2) and (3).

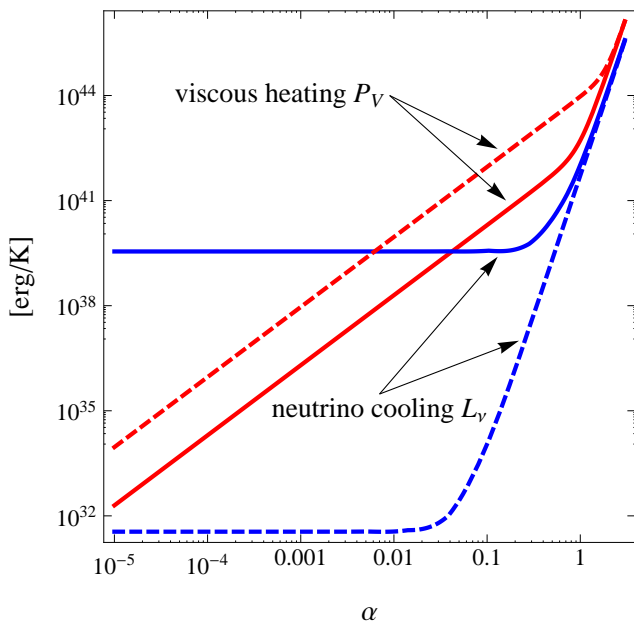


Figure 1: The total neutrino luminosity compared to the viscously dissipated power, as functions of the r-mode amplitude. We show curves for a $1.4 M_\odot$ APR neutron star spinning at half its Kepler frequency and for the two temperatures $T = 10^8 \text{ K}$ (dashed) and $T = 10^9 \text{ K}$ (solid). At lower frequencies the suprathermal regime is only reached at even larger amplitudes [4, 16].

therefore nonlinear processes are even less likely to play a role. In conclusion, the energy that is continuously fed into the mode from the rotational energy reservoir must be completely dissipated to keep the amplitude constant which continuously heats the star.

The complete information on the saturation mechanism is then encoded in the saturation amplitude which can be a general function $\alpha_{\text{sat}}(T, \Omega)$. This function has to vanish at the boundary of the instability region. Due to the strong power law dependence of the corresponding time scales τ_G and τ_V on T and Ω , it drops sharply over a very narrow region, as has been explicitly shown in [4]. For the spindown evolution this narrow boundary region is far less important than the much larger interior of the instability region. In the interior the amplitude will depend much more weakly on T and Ω and we make the

simple power law ansatz

$$\alpha_{\text{sat}} = \hat{\alpha}_{\text{sat}} T^\beta \Omega^\gamma. \quad (22)$$

For instance the semi-analytic expression for the saturation amplitude due to suprathermal bulk viscosity has such a power law dependence on the frequency and proves to be even independent of temperature, i.e. $\beta = 0$ [4]. Since the only temperature dependence in eq. (20) comes from the implicit dependence via α_{sat} , for $\beta = 0$ the spindown evolution is not affected at all by the thermal evolution. This applies in particular to the model employed in [10] where the saturation amplitude is assumed to be constant throughout the instability region, i.e. independent of T and Ω . For a general saturation mechanism the saturation amplitude could be a more complicated function, but as in the analysis of the instability boundary [3] the above form should hold at least locally in different regions in the T - Ω space.

To analyze the above equations it is useful to introduce characteristic evolution time scales

$$\tau_\alpha \equiv -\alpha \left(\frac{d\alpha}{dt} \right)^{-1}, \quad \tau_\Omega \equiv -\Omega \left(\frac{d\Omega}{dt} \right)^{-1}, \quad \tau_T \equiv -T \left(\frac{dT}{dt} \right)^{-1}. \quad (23)$$

A young compact star is born in a core bounce supernova with a large temperature $T > 10^{11} \text{ K}$. We will assume that the initial frequency is above the minimum frequency of the instability region [3]. Initially $\tau_T \sim T^{-(\theta-v-1)}$ is small so that the star cools very fast due to neutrino emission and quickly enters the instability region. There by definition $|\tau_G| < \tau_V|_{\alpha=0}$ and (while the star cools further) the r-mode will grow with time scale $\tau_\alpha \approx \tau_G$. For a compact star spinning with a millisecond period this scale is of the order of seconds, so that the amplitude quickly grows until it is saturated at some α_{sat} . From this point on the fast evolution of α stops and it changes slowly with temperature and frequency. Since cooling is initially very quick but slows down considerably at lower temperatures, at some point the temperature-independent dissipation eq. (19) required to saturate the mode will dominate. The important question for the evolution is then if the spindown or the temperature change is faster. To see this let us analyze the behavior when temperature change due to dissipative heating (neglecting neutrino emission) $\tau_T^{(H)}$ is

faster than the spindown, i.e. $\tau_T^{(H)} < \tau_\Omega$. This condition yields a relation for the angular velocity of the star which introducing the Kepler frequency $\Omega_K = \frac{4}{9}\sqrt{2\pi G\rho_0}$ can be written in the form

$$\frac{\Omega}{\Omega_K} > \frac{27}{8\pi} \sqrt{\frac{\tilde{C}_V}{\tilde{I}(1-Q\alpha_{\text{sat}}^2)} \frac{R}{R_S} \frac{\Lambda_{\text{QCD}}^4}{\bar{\rho}}} \left(\frac{T}{\Lambda_{\text{QCD}}}\right)^{v+1} \xrightarrow{v=1} \text{const} \frac{T}{\Lambda_{\text{QCD}}}, \quad (24)$$

where in the second line we use the fact that for dense matter in general the temperature exponent arising in the specific heat eq. (3) obeys $v \geq 1$, and larger values make the right hand side even smaller. For a compact star the constant is $O(1)$, since the dimensionless parameters \tilde{C}_V and \tilde{I} are normalized to also be $O(1)$, the characteristic scale for the average energy density $\bar{\rho}$ of strongly interacting matter is Λ_{QCD}^4 , the radius of a neutron star is close to its Schwarzschild radius $R_S = 2GM$ and the root further decreases deviations from unity. However, since a compact star is a degenerate system, after a short time it reaches a temperature where $T/\Lambda_{\text{QCD}} \lesssim O(10^{-3})$. Therefore, taking into account the $O(1)$ prefactor, the viscous heating should be faster than the spindown for frequencies $\Omega/\Omega_K \gtrsim 10^{-2}$. Since r-modes are only present within the instability region, this should be compared to the minimum of the instability region Ω_{min} , for which a semi-analytic expression is given in [3]. There it was shown that this minimum is extremely insensitive to the microscopic details which yields a general limit of roughly $\Omega_{\text{min}}/\Omega_K \gtrsim 1/20$. Therefore, at r-mode saturation within the instability region the dissipative heating is always faster than the spindown. Note that this conclusion is generic and to leading order independent of both the saturation amplitude and the composition of the star.

IV. SEMI-ANALYTIC SOLUTION OF THE R-MODE EVOLUTION

A. Endpoint of the evolution

Since for a compact star the thermal evolution is faster than the spindown, the evolution of the star should follow a curve $\Omega_{hc}(T)$ where it is always thermally in a steady state where neutrino cooling equals dissipative heating $L_\nu + P_G = 0$ [24]. With the semi-analytic expressions eqs. (4) and (8) this equation can be solved explicitly and yields for the dominant $m = 2$ r-mode

$$\Omega_{hc}(T) = \left(\frac{3^8 5^2}{2^{15}} \frac{\tilde{L} \Lambda_{\text{QCD}}^{9-\theta} T^{\theta-2\beta}}{\tilde{J}^2 \Lambda_{\text{EW}}^4 G M^2 R^3 \hat{\alpha}_{\text{sat}}^2} \right)^{1/(8+2\gamma)}. \quad (25)$$

The evolution should therefore follow this curve until the star leaves the instability region. As can be seen in

fig. 2, the boundary of the instability region of a neutron star has different segments: a low-temperature boundary outside of which shear viscosity damps the mode and an intermediate-temperature boundary where bulk viscosity is the dominant damping mechanism. Since the bulk viscosity features a resonant behavior and decreases again at very large temperatures $T \gtrsim 10^{11}$ K, there is a third high-temperature boundary above which the r-mode is unstable (see fig. 3 of [3]), but for neutron stars this segment is quite likely physically irrelevant since the star cools below it quickly. Semi-analytic expressions for these segments of the boundary of the instability region have been derived in [3]. The form of the boundary depends strongly on the form of matter [30, 31]. When exotic forms of matter are present then in the relevant temperature regime there are so called stability windows, caused by the resonant behavior of the bulk viscosity of the corresponding phase, where the star is stable against developing an r-mode up to large frequencies (see fig. 3 of [3]). In case the steady-state curve formally lies in such a stability window it would clearly be irrelevant for the spindown⁴. Then the evolution can take a long time, since the strong heating can push the star out of the instability region before the r-mode reaches a large amplitude, and other spindown sources will likely dominate. Therefore we will restrict ourselves here to the case of pure neutron stars. The general evolution for different forms of matter will be discussed elsewhere.

In the case of neutron stars the intermediate-temperature boundary of the instability region has a steeper slope than the steady state curve which thereby can only intersect the low-temperature boundary. In the case of a neutron star the low-temperature boundary $\Omega_{lb}(T)$ is determined by the condition $\tau_S = \tau_G$ and the corresponding semi-analytic solution is [3]

$$\Omega_{lb}(T) = \left(\frac{3^8 5^3}{2^{17} \pi} \frac{\tilde{S} \Lambda_{\text{QCD}}^{3+\sigma}}{\tilde{J}^2 G M^2 R^3 T^\sigma} \right)^{1/6}. \quad (26)$$

Equating eqs. (25) and (26), the final angular velocity Ω_f where the evolution leaves the instability region is given by

$$\Omega_f = \left(\left(\frac{3^8 5^3}{2^{17} \pi} \right)^{\theta+\sigma-2\beta} \left(\frac{4\pi}{5} \right)^\sigma \times \frac{\tilde{S}^{\theta-2\beta} \tilde{L}^\sigma \Lambda_{\text{QCD}}^{3\theta+9\sigma-6\beta-2\beta\sigma}}{\left(\tilde{J}^2 G M^2 R^3 \right)^{\theta+\sigma-2\beta} \Lambda_{\text{EW}}^{4\sigma} \hat{\alpha}_{\text{sat}}^{2\sigma}} \right)^{1/(6\theta+8\sigma+2\gamma\sigma-12\beta)}, \quad (27)$$

and the corresponding temperature T_f reads

⁴ As just noted, for standard neutron stars the corresponding stability window lies at very large temperatures $T > 10^{10}$ K where the neutrino cooling still strongly dominates.

$$T_f = \left(\left(\frac{3^8 5^3}{2^{17} \pi} \right)^{2+2\gamma} \left(\frac{5}{4\pi} \right)^6 \right. \quad (28)$$

$$\times \frac{\tilde{S}^{8+2\gamma} \Lambda_{\text{EW}}^{24} \Lambda_{\text{QCD}}^{-30+6\theta+8\sigma+6\gamma+2\gamma\sigma} \hat{\alpha}_{\text{sat}}^{12}}{\tilde{L}^6 \left(\tilde{J}^2 G M^2 R^3 \right)^{2(1+\gamma)}} \left. \right)^{1/(6\theta+8\sigma+2\gamma\sigma-12\beta)}$$

Note that, if we had used a different steady-state curve $\Omega_{hc}^{(S)}$ where the heating comes only from shear viscosity, as assumed in [10], or if we had included the bulk viscosity as well, the rest of the evolution could be very different, but we would have obtained exactly the same result for the endpoint eqs. (27) and (28) of the evolution. This surprising feature comes about since the shear viscosity is strongly dominant compared to the bulk viscosity on the left boundary and this boundary is precisely defined by the condition $\tau_S = \tau_G$ which implies that dissipated power equals the power radiated in gravitational waves $P_S = P_G$. In this sense the result eq. (27) is universal and does not depend on assumptions about the dissipative aspects of the saturation mechanism.

The above expressions involve the star constants given in tab. II. In order to give these expressions in a more physical form we write them relative to a fiducial reference model chosen as a $1.4 M_\odot$ neutron star with an APR equation of state [19] given in the first row of tab. II and denoted by a subscript “fid”. In case of a constant, T - and Ω -independent, saturation amplitude [10] $\beta = \gamma = 0$ this gives for a *standard* neutron star (NS) with shear viscosity due to leptonic processes and neutrino emission due to modified Urca reactions

$$T_f^{(NS)} \approx (1.26 \cdot 10^9 \text{ K}) \left(\frac{\tilde{S}}{\tilde{S}_{\text{fid}}} \right)^{3/23} \left(\frac{\tilde{L}}{\tilde{L}_{\text{fid}}} \right)^{-9/92} \left(\frac{\tilde{J}}{\tilde{J}_{\text{fid}}} \right)^{-3/46}$$

$$\times \left(\frac{M}{1.4 M_\odot} \right)^{-3/46} \left(\frac{R}{11.5 \text{ km}} \right)^{-9/92} \alpha_{\text{sat}}^{9/46}, \quad (29)$$

$$f_f^{(NS)} \approx (61.4 \text{ Hz}) \left(\frac{\tilde{S}}{\tilde{S}_{\text{fid}}} \right)^{3/23} \left(\frac{\tilde{L}}{\tilde{L}_{\text{fid}}} \right)^{5/184} \left(\frac{\tilde{J}}{\tilde{J}_{\text{fid}}} \right)^{-29/92}$$

$$\times \left(\frac{M}{1.4 M_\odot} \right)^{-29/92} \left(\frac{R}{11.5 \text{ km}} \right)^{-87/184} \alpha_{\text{sat}}^{-5/92}. \quad (30)$$

First it is interesting to note that all these expressions depend neither on the specific heat nor directly on the bulk viscosity of the considered form of matter. The latter is at first sight surprising since the bulk viscosity is the dominant dissipation mechanism at high temperatures and low amplitudes. But during the spindown evolution the dissipation is dominated by the appropriate saturation mechanism while the amount of dissipation is according to eqs. (11) and (19) determined entirely by gravitational physics. This is particularly favorable since it eliminates the complications arising from the fact that the damping due to bulk viscosity requires

the density fluctuation of the r-mode eq. (12) which is only non-vanishing to second order in Ω [15] and involves significant uncertainties. Even more striking is the extreme insensitivity of these result to the remaining microphysics included in the constants \tilde{S} and \tilde{L} . The neutrino emissivity constant \tilde{L} , in particular, depends on poorly known strong interaction corrections to the weak processes [18]. Yet, the remarkably small power $5/184$ arising in the important expression for the final angular velocity $\Omega_f^{(NS)}$ almost eliminates this uncertainty. The dependence of $\Omega_f^{(NS)}$ on the shear viscosity constant \tilde{S} is somewhat stronger, but \tilde{S} is dominated by electromagnetic leptonic processes [32] that are well under theoretical control⁵ and depends on the equation of state only via the lepton densities. The dependence on the parameters \tilde{J} , M and R which encode macroscopic properties of the star is stronger, but they vary only within narrow margins. This insensitivity to the underlying parameters is similar to the case of the minimum of the instability region [33] analyzed previously in [3], yet it is fortunately even more pronounced in the physically important case eq. (30). The most striking feature of these expressions, however, is that the insensitivity extends even to the dependence on α_{sat} , which is theoretically uncertain by many orders of magnitude [4, 24, 26, 27] and therefore represents the main uncertainty in the analysis. Here the similarly small power $5/92$ dramatically reduces this dependence and thereby allows a quantitative comparison with observational data below.

To get an idea of the uncertainty in $f_f^{(NS)}$ we estimate the error ranges of the individual parameters by symmetric logarithmic error bands - i.e. we allow for the corresponding parameter to be smaller or larger than the APR reference star by a given factor. The shear viscosity parameter \tilde{S} due to leptonic processes [32] is uncertain within a factor of two of \tilde{S}_{fid} and the neutrino emissivity parameter \tilde{L} due to modified Urca processes [18] within an order of magnitude of \tilde{L}_{fid} . For \tilde{J} we have rigorous limits eq. (14). An upper limit for the mass of a neutron star is $\lesssim 2.5 M_\odot$ and an upper limit for the radius of a star rotating with millisecond periods about $\lesssim 15 \text{ km}$. Since the upper bound for \tilde{J} is for a constant density profile which is far from the situation in a neutron star and, due to cancellations, the dependence on the mass and radius turns out to be significantly weaker than these individual individual errors suggest, see table III below, we consider half the above ranges for the individual logarithmic uncertainties for \tilde{J} , M and R as a more realistic estimate. Under the assumption that these errors are independent we find

⁵ There is a hadronic contribution to the shear viscosity as well but the latter is strongly subleading at temperatures relevant to young neutron stars due to the different power law dependence.

$$f_f^{(NS)} \approx (61.4 \pm 9.4) \text{ Hz } \alpha_{\text{sat}}^{-5/92}. \quad (31)$$

We want to stress that this is just an estimate of the likely error range and not a statistical measure of well defined significance.

Different classes of compact stars, containing other phases of dense matter with different low energy degrees of freedom, feature different values for the exponents in eqs. (2) and (3) and can lead to qualitatively different behavior. An example is a heavy star where direct Urca reactions are kinematically allowed in an inner core and the parameters change according to table II which increases the final frequency beyond the above error range. When exotic forms of matter are present, like hyperon or quark matter, the enhanced dissipation of these phases leads to stability windows [3, 30, 31, 34]. In this case the boundary of the stability window in the relevant temperature regime is determined by the bulk viscosity of the exotic phase, so that eqs. (27) and (28) are not valid. The steady state curve then ends at a higher frequency due to the instability window where the star leaves the unstable regime and cools until it reaches the lower boundary of the stability window. Since at these lower temperatures r-mode heating dominates neutrino cooling the star is repeatedly pushed out of the instability region once its amplitude becomes large and the residual spindown takes much longer [35, 36]. The important point is however, that the final frequency which is in this case given by the minimum of the instability region and for which a similarly precise semi-analytic result exists [3] is systematically larger for exotic forms of matter since the strong bulk viscosity of the exotic phase dominates the shear viscosity down to lower temperatures. Therefore, the above expressions eqs. (30) and (31) provide lower bounds for the frequency to which an arbitrary compact star can be spun down due to the r-mode instability.

B. Dynamical evolution and time scales

Next let us actually solve the evolution equations to obtain the corresponding evolution time scales. The initial cooling time in the stable regime before the evolution enters the instability region t_{sc} results from solving the thermal equation eq. (18), in the absence of viscous heating, down to the temperature determined by the semi-analytic expression for the intermediate-temperature boundary of the instability region given in [3]. The result reads

$$t_{sc} = \frac{1}{\theta - \nu - 1} \left(\frac{3^3 5^2}{2^{12} 7 \pi \kappa^2} \right)^{(\theta - \nu - 1)/\delta} \times \left(\frac{\tilde{V}_m^{\theta - \nu - 1} \tilde{C} \Lambda_{\text{QCD}}^{9(\theta - \nu - 1) - 5\delta} R^{\theta - \nu - 1}}{\tilde{L}^\delta \Lambda_{\text{EW}}^{4(\theta - \delta - \nu - 1)} (\tilde{J}^2 G M^2 \Omega_i^4)} \right)^{1/\delta} \quad (32)$$

in terms of the initial angular velocity Ω_i and depends both on the bulk viscosity and the specific heat. For a standard neutron star with shear viscosity due to leptonic processes and neutrino emission due to modified Urca reactions this gives

$$t_{sc}^{(NS)} \approx (7.83 \cdot 10^{-2} \text{ s}) \left(\frac{\tilde{V}}{\tilde{V}_{\text{fid}}} \right) \left(\frac{\tilde{J}}{\tilde{J}_{\text{fid}}} \right)^{-2} \left(\frac{\tilde{C}}{\tilde{C}_{\text{fid}}} \right) \left(\frac{\tilde{L}}{\tilde{L}_{\text{fid}}} \right)^{-1} \times \left(\frac{M}{1.4 M_\odot} \right)^{-2} \left(\frac{R}{11.5 \text{ km}} \right) \left(\frac{f_i}{\text{kHz}} \right)^{-4}. \quad (33)$$

This time is so short compared to the subsequent r-mode evolution that it can safely be neglected.

The spindown time t_{sd} is obtained by solving the frequency equation (20) in the saturated regime. Even though for r-mode emission the spindown evolution is coupled to the thermal evolution when the saturation amplitude is temperature-dependent the knowledge of the path of the evolution within the instability region, determined by the analytic steady state solution eq. (25) of the thermal equation, allows us to derive the effective spindown equation. Inserting (the inverse of) the steady state relation eq. (25) into the spindown equation (20) we find

$$\frac{d\Omega}{dt} = - \frac{2^{17} \pi \tilde{J}^2 G M R^4}{3^7 5^2 \tilde{I}} \left(\frac{2^{15} \tilde{J}^2 G \Lambda_{\text{EW}}^4 M^2 R^3}{3^8 5^2 \tilde{L} \Lambda_{\text{QCD}}^{9-\theta}} \right)^{\frac{2\beta}{\theta-2\beta}} \times \hat{\alpha}_{\text{sat}}^{\frac{2\theta}{\theta-2\beta}} \Omega^{n_{rm}} \quad (34)$$

I.e. despite the coupling with the thermal evolution, the spindown equation takes a standard power law form [6], yet with an *effective* braking index

$$n_{rm} = \frac{(7+2\gamma)\theta+2\beta}{\theta-2\beta} = 7 \left(\frac{1+2\gamma/7+2\beta/(7\theta)}{1-2\beta/\theta} \right) \quad (35)$$

The correction factor in parentheses changes the braking index from the canonical value which is 7 for r-mode emission. The correction factor takes the value 1 for a constant saturation amplitude ($\beta = \gamma = 0$), but for general β and γ it deviates from 1 and lowers the braking index, since for proposed saturation mechanisms [4, 23–25] $\beta, \gamma < 0$. Using these values we find that the correction factor can decrease the braking index to nearly half of its canonical value and therefore has a significant impact on the spindown evolution. E.g. for mode coupling with damping due to shear viscosity [25], where $\beta = -4/3$ and $\gamma = -2/3$, it reduces to $n_{rm}^{(mc)} = 4$. This is rather close to the canonical value of 3 for electromagnetic dipole radiation. Therefore, it should be harder than expected to distinguish these different spindown scenarios based on their braking indices. Actually, an even lower value is obtained for the recently proposed scenario that the

cutting of superconducting flux tubes by superfluid vortices can saturate r-modes [37], where $\beta = 0$, $\gamma = -3$. In this case the braking index takes the extreme value $n_{rm}^{(fc)} = 1$, which means that the spindown is not even power-like but logarithmic and the general solution given below does not apply. However, the spindown evolution decouples in this case and can be easily solved. The case of the suprathreshold bulk viscosity [4] is more complicated and will be studied elsewhere, since the large amplitude enhancement of the neutrino emissivity would here be relevant to determine the effective braking index. As discussed before such effects are not relevant unless suprathreshold damping saturates the mode, which is not the case for standard bulk viscosity from a neutron star core.

Even though the spindown evolution is coupled to the thermal evolution when the saturation amplitude is temperature-dependent, the knowledge of the path of the evolution within the instability region at saturation eq. (25) allows us to solve the spindown equation (34) fully analytically for the power-law parameterization eq. (22) which gives⁶

$$\Omega(t) = \left(\Omega_i^{-\frac{2(3+\gamma)\theta+4\beta}{\theta-2\beta}} + \frac{2^{18}\pi(3+\gamma)\theta+2\beta}{375^2} \frac{\tilde{J}^2 G M R^4}{\tilde{I}} \right)^{-\frac{\theta-2\beta}{2(3+\gamma)\theta+4\beta}} \times \left(\frac{2^{15}}{385^2} \frac{\tilde{J}^2 G \Lambda_{\text{EW}}^4 M^2 R^3}{\tilde{L} \Lambda_{\text{QCD}}^{9-\theta}} \right)^{\frac{2\beta}{\theta-2\beta}} \hat{\alpha}_{\text{sat}}^{\frac{2\theta}{\theta-2\beta}} (t - t_i) \quad (36)$$

An interesting aspect of this expression is that for a frequency-independent saturation amplitude it does not depend on the cooling behavior which reflects the previous observation that the thermal and spindown evolutions decouple in this case. Eq. (36) has two limits, at early times where the first term in the parenthesis dominates and at late times where the second dominates. I.e. initially the amplitude hardly changes whereas at late times the evolution becomes independent of the initial conditions. The semi-analytic temperature evolution at saturation is then obtained by inserting the frequency solution eq. (36) in the inverse of the steady state curve eq. (25). In the late time limit we find

⁶ As noted before, in general the saturation amplitude might only locally have the power law from eq. (22). In this case there are different regions in T - Ω space where the evolution is locally described by eq. (36) and one would in principle have to solve the evolution stepwise with appropriate initial conditions. Since the spindown strongly slows down at late times and becomes then effectively independent of the initial conditions (the first term in the parenthesis of eq. (36) can be neglected), at late times eq. (36) is a good approximation even in the general case. It is sufficient at late times to consider the power law dependence of the saturation amplitude realized in the final evolution segment and it is irrelevant that the dependence was different early in the evolution.

$$T(t) \approx \left(\left(\frac{3^7 5^2}{2^{18} \pi} \frac{\theta - 2\beta}{(3 + \gamma)\theta + 2\beta} \frac{\tilde{I}}{\tilde{J}^2 G M R^4 t} \right)^{8+2\gamma} \times \left(\frac{2^{15}}{385^2} \frac{\tilde{J}^2 G \Lambda_{\text{EW}}^4 M^2 R^3}{\tilde{L} \Lambda_{\text{QCD}}^{9-\theta}} \right)^{2(3+\gamma)} \hat{\alpha}_{\text{sat}}^{-4} \right)^{\frac{1}{2(3+\gamma)\theta+4\beta}} \quad (37)$$

For a standard neutron star in particular we find for the constant saturation model in the late time limit $\Omega(t) \sim T(t) \sim t^{-1/6}$.

For the spindown time we find then in terms of the gravitational time scale eq. (4) evaluated at the final frequency

$$t_{sd} = -\frac{\theta - 2\beta}{4(3 + \gamma)\theta + 8\beta} \frac{\tau_G(\Omega_f)}{Q \alpha_{\text{sat}}^2(\Omega_f)} \left(1 - \left(\frac{\Omega_f}{\Omega_i} \right)^{\frac{2(3+\gamma)\theta+4\beta}{\theta-2\beta}} \right) \xrightarrow{\Omega_f \ll \Omega_i} -\frac{C \Omega_f}{6 \dot{\Omega}_f} \quad (38)$$

where the dependence on the saturation model enters only via the constant prefactor

$$C \equiv \frac{1 - 2\beta/\theta}{1 + \gamma/3 + 2\beta/(3\theta)} = \frac{6}{n_{rm} - 1} \quad (39)$$

which takes the value 1 for a constant saturation amplitude ($\beta = \gamma = 0$). For general β and γ it deviates from 1, but for proposed saturation mechanisms [4, 23–25] $\beta, \gamma < 0$ so that up to small corrections in Ω_f/Ω_i this simply increases the spindown time compared to a constant saturation amplitude by a constant factor. Since in hadronic matter $\theta = 8$ these corrections are modest⁷ and for the exponents predicted by proposed saturation mechanisms [4, 23–25] it amounts at most to a factor two. E.g. in case of dissipation due to suprathreshold bulk viscosity [4] the spindown time is longer compared to the saturation model with a constant amplitude by a factor of 9/5. Taking into account our ignorance of the complicated r-mode saturation physics this simple and moderate dependence is most welcome.

The above expression eq. (38) looks similar to the relation between the spindown time for other spindown mechanisms, like magnetic dipole radiation or gravitational wave emission due to deformations, and the characteristic pulsar time scale $-\Omega_0/\dot{\Omega}_0$ [6]. Yet, the important point to note here is, that Ω_f and $\dot{\Omega}_f$ are the values before the star leaves the instability region which can be very different from the observed values Ω_0 and $\dot{\Omega}_0$ if the observation is performed after the star has left the instability region. The characteristic feature of the r-mode

⁷ This holds in general degenerate fermionic phases where $\theta \geq 6$.

mechanism, namely that it operates only for a finite time interval, renders the r-mode spindown time completely independent of the characteristic pulsar time scale and allows the former to be orders of magnitude smaller, since the spindown rate can strongly drop from a large r-mode rate to a much lower rate of other spindown mechanisms at the boundary of the instability region.

Inserting the expression for the final frequency eq. (30) into eq. (38) this yields for the constant saturation model in case of a standard neutron star and for $\Omega_f \ll \Omega_i$

$$t_{sd}^{(NS)} \approx (12.3 \text{ y}) \left(\frac{\tilde{S}}{\tilde{S}_{\text{fid}}} \right)^{-18/23} \left(\frac{\tilde{L}}{\tilde{L}_{\text{fid}}} \right)^{-15/92} \left(\frac{\tilde{J}}{\tilde{J}_{\text{fid}}} \right)^{-5/46} \times \left(\frac{\tilde{I}}{\tilde{I}_{\text{fid}}} \right) \left(\frac{M}{1.4 M_{\odot}} \right)^{41/46} \left(\frac{R}{11.5 \text{ km}} \right)^{-107/92} \alpha_{\text{sat}}^{-77/46}. \quad (40)$$

Here the dependence on the parameters is stronger than for the endpoint of the evolution eqs. (27) and (28), so that the duration is considerably more uncertain. In particular it is very sensitive to the saturation amplitude α_{sat} . If α_{sat} becomes too small this time scale is so long that other spindown mechanisms will dominate, as is clear from the sizable observed spindown rate of young pulsars [38]. Employing the bounds eqs. (13) and (14) as well as the full uncertainty ranges for the other underlying parameters discussed before to estimate the uncertainty in the final frequency eq. (31) we find that the spindown time could be smaller or larger by nearly an order of magnitude.

V. SPINDOWN OF YOUNG PULSARS

A. Comparison of analytic and numeric results

The results for the evolution of the $1.4 M_{\odot}$ neutron star in temperature-angular velocity space is shown in fig. 2 for different values of the initial rotation angular velocity and the saturation amplitude. As can be seen the numerical solution given by the solid curves perfectly confirms the above picture. The star initially cools until it reaches the instability region, where the r-mode amplitude starts to grow. Once the amplitude is significant the star starts spinning down but since the spindown time τ_{Ω} is much longer than the cooling time τ_T , the star cools further until it reaches the steady state curve⁸ where the fast temperature evolution is stopped and the star evolves along the steady state curve on the longer time scale τ_{Ω} .

⁸ For the largest saturation amplitudes the evolution reaches the steady state temperature before its amplitude has saturated. Therefore, as can be seen from the $\alpha_{\text{sat}} = 1$ curve in fig. 2, the star “undercools” to lower temperatures and then reheats back to the steady state curve once the saturation amplitude is reached.

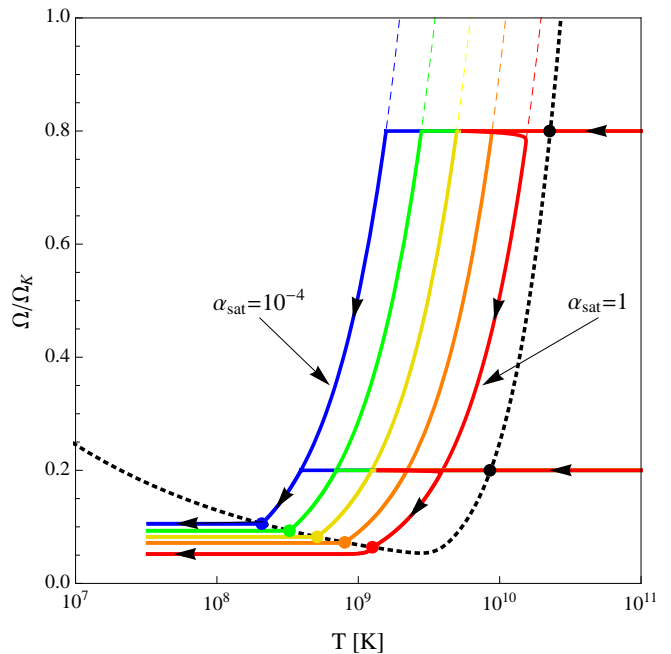


Figure 2: The spindown evolution of a young $1.4 M_{\odot}$ neutron star with an APR equation of state [19] in temperature-angular velocity space. The boundary of the instability region of the fundamental $m = 2$ r-mode is shown by the dotted curve. The dashed curves (which are mostly hidden underneath the solid curves) represent the steady state eq. (25) where heating equals cooling and are given for different r-mode amplitudes ranging from $\alpha_{\text{sat}} = 10^{-4}$ (left) to $\alpha_{\text{sat}} = 1$ (right). The solid lines show the numerical solution of the evolution equations for two fiducial initial spin frequencies $\Omega = 0.8 \Omega_K$ and $\Omega = 0.2 \Omega_K$. As can be seen, after an initial cooling phase the evolution simply merges on the appropriate steady state curve and follows it to the edge of the instability region. The dots denote the semi-analytic results for the points of the spindown evolution where the star enters and leaves the instability region, eqs. (29) and (30).

Consequently, the evolution is completely independent of the initial amplitude α_{min} required to start the growth in eq. (16). Such initial perturbations will clearly be present immediately after the creation of the neutron star following a core bounce. As anticipated, the numerical solution also proves that the evolution is to very good accuracy independent of the initial frequency unless it is very close to the final frequency. Therefore, similar to the thermal evolution, the spindown evolution completely loses its memory of the initial conditions at sufficiently late times. The saturation amplitude in contrast provides the dominant uncertainty for the evolution and the trajectory is shown for a range of possible saturation amplitudes. Larger values lead to stronger dissipative reheating and therefore spin down the star at larger temperatures so that the evolution leaves the instability region at lower frequencies closer to the minimum of the instability region. The dots are obtained from the analytic expressions eqs. (29) and (30) which agree with the numerical solution. Note

again that we neglect other spindown mechanisms like magnetic dipole radiation in this work which would speed up the evolution and continue the magnetic spindown after the star leaves the r-mode instability region.

In [10] the evolution was artificially stopped at a temperature of 10^9 K since superfluidity and non-perfect fluid effects were expected to invalidate the analysis below. We do not follow this ad hoc prescription here since it is not likely that these effects have such a big influence on the spindown evolution for the following reasons: One important effect of superfluidity is to affect beta equilibration. Around the critical temperature it is enhanced due to pair breaking, but at temperatures far below and small oscillation amplitudes beta equilibration processes are strongly suppressed. Since the superfluid gap depends strongly on density the entire star may not be gapped at such temperatures and in this case in part of the star the weak interactions would hardly be affected and the corresponding parameters \tilde{L} and \tilde{V} would only moderately be reduced. Even more, as has recently been shown in [17], superfluidity does not suppress weak processes at all at sufficiently large amplitudes that are within the range we study here. Superfluidity can also lead to an additional source of dissipation via mutual friction. In contrast to the earlier generic analysis referred to in [10], the later dedicated r-mode analysis [39] showed that it is unlikely that mutual friction has such a dramatic impact on the r-mode instability. In [40] this effect was studied, taking into account the large uncertainties in pairing and the microscopic drag parameter. It was found that depending on these uncertainties the effect can range from the unlikely extreme that the r-mode is completely suppressed below a certain temperature to a nearly negligible impact on the instability region compared to the ungapped case. Therefore, it is interesting to study the present case of standard dissipation sources in detail, since it sets the limit on the frequency to which r-modes can spin down a star as well as on the emitted gravitational wave signal, as discussed below. Any additional dissipation source will reduce the r-mode instability and correspondingly lead to larger final spin frequencies and a reduced gravitational wave emission.

Fig. 3 shows the evolution of the angular velocity as a function of time. As predicted by eq. (40), the spindown time increases strongly with decreasing saturation amplitude. The points show that the semi-analytic results for this time again agree with the numerical solution⁹. Here we are mainly interested in the spindown aspects

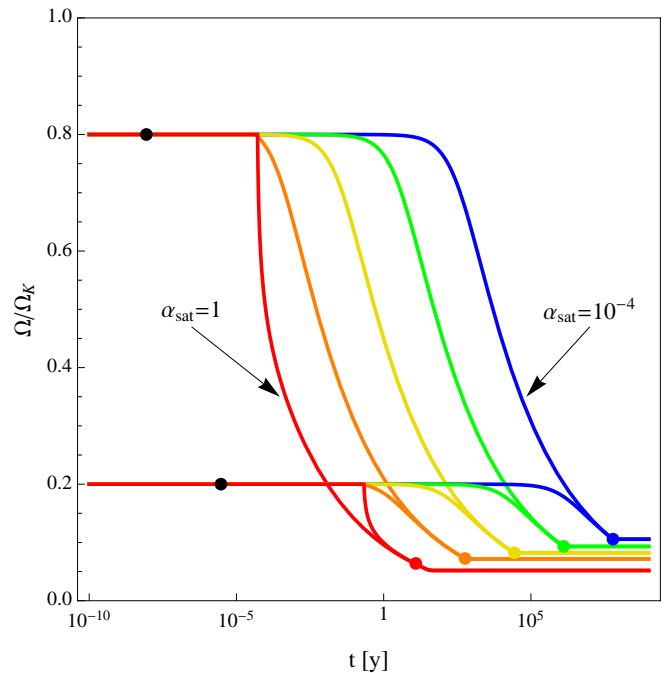


Figure 3: The spindown evolution of a young neutron star. The solid lines show the evolution of a $1.4 M_{\odot}$ star with an APR equation of state and for different constant saturation amplitudes ranging from $\alpha_{\text{sat}} = 1$ (left) to $\alpha_{\text{sat}} = 10^{-4}$ (right). The dots denote the analytic results eq. (33) respectively eqs. (40) and (30) for the point of the spindown evolution where the star enters and leaves the instability region.

and only note that as far as the thermal evolution is concerned the r-mode effectively causes a delay in the cooling [41]. This is significant initially, but, since the cooling slows down strongly, it is irrelevant at much later times $t \gg t_{sd}$.

Table III lists the semi-analytic results for a range of saturation amplitudes for two different neutron stars - the previously discussed standard star with a canonical mass of $1.4 M_{\odot}$ and, motivated by the recent observation [42], also a heavy $2.0 M_{\odot}$ star. Strikingly the final frequency proves nearly independent of the mass, and is far less sensitive than eq. (30) naively suggests. This is apparently caused by cancellations due to the implicit mass dependence of the radius and of the parameters \tilde{J} , \tilde{S} and \tilde{L} . Despite the explicit normalizations in table I these parameters still have a significant implicit dependence on M and R via the density profile of the star. Correspondingly, whereas the dependence on microscopic material properties is explicitly given by the semi-analytic expressions eqs. (27) to (40), the dependence on star properties like the mass and radius is not properly reflected by the explicit dependencies alone but the additional implicit dependence via the averaged quantities in table I is cru-

⁹ Note that the spindown overshoots at large amplitude since it takes time for the amplitude to decay and the spindown continues during this period, as can be seen from the lowest curve which drops below the dot so that the final frequency lies somewhat below the instability region. This is mainly an artifact of the simplified model which keeps the amplitude constant until the instability boundary is reached. In reality with an explicit saturation mechanism the amplitude has to vanish at the boundary in the static limit, so it must start decreasing inside the instability

region, see [4].

α_{sat}	T_f [10^8 K]	Ω_f/Ω_K	f_f [Hz]	t_{sd} [y]
1	12.6 (13.9)	0.064 (0.049)	61.4 (60.3)	12.3 (9.4)
0.1	8.02 (8.88)	0.073 (0.056)	69.5 (68.4)	582 (445)
10^{-2}	5.11 (5.66)	0.082 (0.063)	78.8 (77.5)	$2.75 (2.10) \cdot 10^4$
10^{-3}	3.26 (3.61)	0.093 (0.072)	89.3 (87.8)	$1.30 (0.99) \cdot 10^6$
10^{-4}	2.08 (2.30)	0.106 (0.081)	101.2 (99.5)	$6.11 (4.68) \cdot 10^7$

Table III: Dependence of the results obtained from the semi-analytic expressions for the characteristic quantities eqs. (29), (30) and (40) of the spindown evolution for neutron star with an APR equation of state on the saturation amplitude α_{sat} . We give in each case results for both a standard $1.4 M_\odot$ star and a heavy $2.0 M_\odot$ star next to it in parentheses. At the smallest amplitudes the given spindown times t_{sd} should not be relevant since they would be so long that the neglected magnetic spindown should dominate and spin down the star on much shorter time scales.

cial. The initial cooling time before the star enters the instability region is amplitude independent and yields for a star spinning at the Kepler frequency the small values $t_{sc} = 96.4$ (55.1) ms, which rise to a few hours for frequencies at the lower end of the instability region, which is indeed negligible compared to the long spindown times. The left part of table V finally compares the spindown observables for different stars at a fixed amplitude $\alpha_{\text{sat}} = 1$. We see that, when direct Urca processes are allowed, the final temperature is significantly lower due to the enhanced neutrino cooling. Since the instability region shrinks at lower temperatures the final frequency is higher and the spindown time is correspondingly shorter.

1. Saturation model dependence

Let us now discuss the influence of different saturation models $\alpha_{\text{sat}}(T, \Omega)$. Since in the general case eq. (22) the amplitude varies over the instability region and the coefficient $\hat{\alpha}_{\text{sat}}$ is a dimensionful parameter, we have to find analogous parameter values for $\hat{\alpha}_{\text{sat}}$ to compare saturation models with different values of β and γ among each other and with the constant model discussed so far. Since the evolution spends most of the time in the final stages of the spindown evolution it is natural to choose $\hat{\alpha}_{\text{sat}}$ so that different models have a similar amplitude in this stage. If we compare models defined by $\hat{\alpha}_{\text{sat}}$, β and γ that have the same amplitude α_{sat} at the end of the evolution, then they leave the instability region at the same point given by eqs. (27) and (28). This can be easily seen, noting that the conditions $\tau_S = \tau_G$ and $P_S = P_G$ that determine the endpoint depend only on the saturation amplitude $\alpha_{\text{sat}}(T_f, \Omega_f)$ at this point. However, the path within the instability region, determined by the steady state curve eq. (25), and in particular the thermal behavior will depend on β and γ .

Fig. 4 shows a few examples of different saturation models for two different saturation amplitudes $\alpha_{\text{sat}} =$

10^{-4} and $\alpha_{\text{sat}} = 1$ at the end of the evolution. The solid lines are the constant model $\beta = \gamma = 0$ [10] discussed above. The dashed curves show the case of mode coupling with damping of the daughter modes due to shear viscosity in a star with an impermeable crust [25]. In this case $\beta = -4/3$ and $\gamma = -2/3$ but depending on the particular damping mechanism of the daughter modes other dependencies are possible [25]. Since the amplitude is lower at large frequency the dissipative heating is smaller and the steady state curve becomes steeper and the equilibrium is reached at lower temperatures.

The final, and somewhat extreme, example is the recently proposed dissipation due to the cutting of superconducting flux tubes by superfluid vortices when both neutrons and protons pair in a neutron star core [37]. In this case $\beta = 0$, $\gamma = -3$. This moves the steady state curves to even lower temperatures. As discussed before, this gives a braking index of one so that the spindown is not power-like but logarithmic and strongly slowed down. In conclusion, different saturation mechanisms can change both the thermal evolution and the spindown evolution significantly and generically increase the spindown time. However, eq. (27) shows that the observed insensitivity to the microscopic parameters is not strongly altered by the saturation model for realistic values $|\beta|, |\gamma| \ll \theta$.

B. Comparison to pulsar data

The semi-analytic expressions finally allow us to compare our theoretical results to observational data. In most analyses, e.g. for low mass X-ray binaries [30, 31], the observed pulsar frequencies and temperatures are compared to numerical computations of the r-mode instability region. Since the instability boundary is strongly temperature dependent, information on the temperature is required to decide if the star is actually inside the instability region. However, the temperature is unknown for most young pulsars. For stars which spin slow enough that they are clearly below the minimum of the instability region the knowledge of the frequency is enough to rule out that r-mode oscillations are present. However, there is at least one young star which lies above the minimum of the instability region. Therefore, we will here go beyond such a static analysis and take into account the dynamic evolution as well as the frequency eq. (27) where the star actually leaves the instability region.

In addition to the spin frequencies also the spindown rates are known for many young stars. Naturally, this additional information provides a stronger constraint on spindown models. The time derivative of the frequency is readily obtained from eq. (20). Fig. 5 compares the spindown evolution for different saturation amplitudes to the data for young stars that still have a significant spindown rate. As can be seen there is one pulsar J0537-6910 that spins fast enough that it could be within the instability region of a standard neutron star whose min-

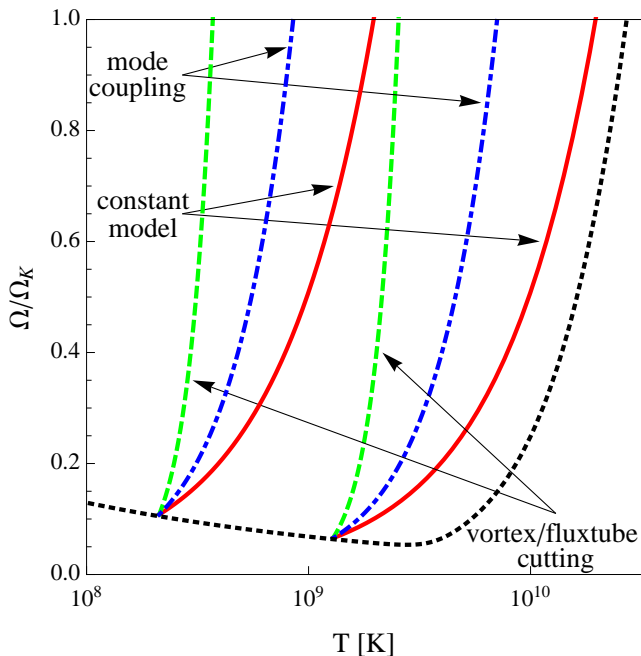


Figure 4: The dependence of the steady-state curve eq. (25) on the saturation model for two different constant saturation amplitudes $\alpha_{\text{sat}}(T_f, \Omega_f) = 10^{-4}$ (left curves) and 1 (right curves) at the end of the evolution. The solid line shows the model with constant amplitude $\beta = \gamma = 0$ [10], the dot-dashed curve shows a mode-coupling model where $\beta = -4/3$ and $\gamma = -2/3$ [25] and the dashed line denotes the case $\beta = 0$, $\gamma = -3$ corresponding to saturation by cutting of superconducting flux tubes by superfluid vortices [37].

imum frequency is denoted by the vertical dotted line to the left¹⁰. Taking into account the dynamical evolution, the additional knowledge of the spindown rate alleviates the uncertainty with respect to the saturation amplitude, since larger amplitudes lead to significantly larger spindown rates. This is shown by the black line which is formed by the semi-analytic results for the endpoints of the evolution and which represents the boundary of the instability region in f - \dot{f} -space. The gray band reflects the uncertainty in the underlying parameters eq. (31). The fastest pulsar J0537-6910 is obviously compatible with being outside of the instability region. We conclude that no observed star lies definitely inside the instability region (see also [23]) which confirms the r-mode scenario for a sufficiently large saturation amplitude resulting in a short spindown time. Moreover, J0537-6910 lies clearly below the line for our APR neutron star and just at the lower edge of the uncertainty band. Therefore, very likely no young star observed so far currently

emits gravitational waves because of the r-mode instability. This conclusion is strengthened by the absence of gravitational wave signals from observed young pulsars - including J0537-6910 - in the latest LIGO data [43]. Unfortunately, the measured braking index of $n \approx -1.5$ for J0537-6910 [44] seems to be strongly affected by the glitch activity of the pulsar [6] and therefore cannot provide conclusive evidence on the current spindown mechanism. For other pulsars the measured braking indices¹¹ $n \lesssim 3$, as shown in fig. 5 for the Crab [6] and the Vela [45] pulsar, already revealed a dominant electromagnetic spindown. For the Crab pulsar this was further strengthened by the LIGO S5 limit [46], showing that it could at most emit a few percent of the rotational energy loss as gravitational waves.

The remarkable aspect of eq. (30) for the final frequency of the spindown is that it is a robust lower bound and is not affected by our ignorance of the star's composition. Although our analysis was performed for a standard neutron star, any additional exotic forms of matter entail enhanced damping so that their instability regions do not extend to such low frequencies. The insensitivity of the final frequency eq. (27) to the underlying parameters, therefore provides a quantitative, universal lower bound given by eq. (31). As a consequence our result shows that the r-mode picture of the spindown of young pulsars presents a viable explanation for the low spin rates of young pulsars if the saturation amplitude is large enough $\alpha_{\text{sat}} \gtrsim 0.01$ to spin down the pulsar in a time $t_{sd} < 10^4$ y. An upper limit for the saturation amplitude $\alpha_{\text{sat}} < 1$ comes from the observed timing data of J0537-6910, as noted in [47], since r-modes would have otherwise spun it down to its current frequency in less than a hundred years which is much shorter than its age estimate [48]. Whereas the r-mode picture yields a direct and quantitative explanation for the maximum observed spin frequency, other mechanisms, like the possibility that all stars are already born with lower frequencies or the subsequent spindown via magnetic dipole radiation, generally only provide probabilistic answers why fast stars with a small initial magnetic dipole moment resulting in a slow spindown could not form. Despite the general trend that according to the dynamo mechanism fast spinning stars feature larger magnetic fields [49], the required spindown evolution studies rely on Monte Carlo population synthesis modeling and involve uncertainties that are to some extent exploited to reproduce the statistical aspects of the observed pulsar distribution [50]. Finally, further indirect evidence for the above r-mode bound comes from pulsars in old and very stable double neutron star binaries which are not recycled and correspondingly should not have experienced any ap-

¹⁰ The analytic result for the minimum of the instability region given in [3] would allow us to estimate also the uncertainties on the minimum frequency, but we refrain from this for better readability.

¹¹ The braking index (see eq. (50)) would be 3 for pure magnetic dipole emission, 5 for spindown via gravitational waves due to an ellipticity of the star [6] and a value ≤ 7 for spindown due to r-modes as discussed above.

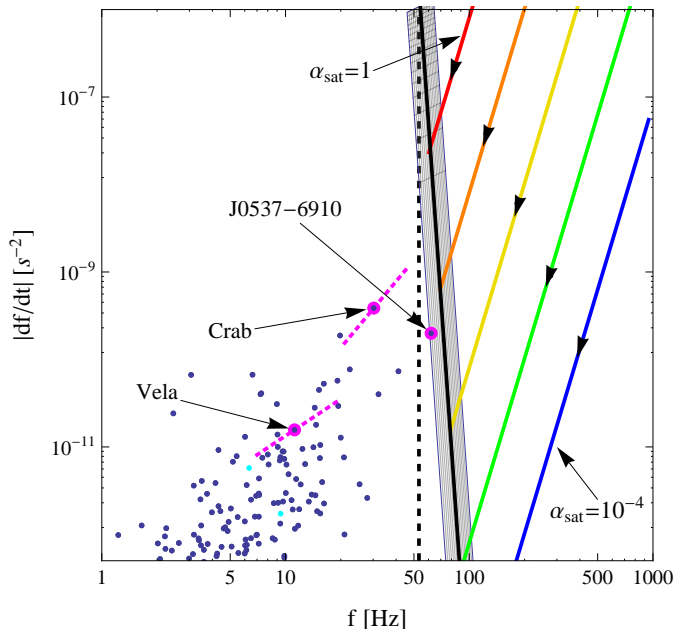


Figure 5: The spindown evolution of a young neutron star compared to observed pulsar data from the ATNF catalog [38]. The solid lines show the evolution of the $1.4 M_{\odot}$ star for different saturation amplitudes ranging from $\alpha_{\text{sat}} = 1$ (top) to $\alpha_{\text{sat}} = 10^{-4}$ (bottom). The vertical dashed line to the left shows the lower frequency boundary of the instability region. The steep solid line is formed by the endpoints of the evolution for different values of α and thereby represents the boundary of the instability region in f - \dot{f} -space, whereas the gray band reflects the error due to the uncertainty in the underlying parameters. The dotted line segments show the current evolution for two stars for which a reliable braking index is available [6, 45].

preciable spin-up during their evolution. The fastest of these, J0737-3039A located in the only known double pulsar system [51], has a frequency of $f \approx 44$ Hz which is still intriguingly close to the quantitative r-mode bound eq. (31).

VI. GRAVITATIONAL WAVE EMISSION

As discussed in the previous section, all presently observed young pulsars are likely outside of the instability region and so should not emit gravitational radiation due to r-modes. Nevertheless, it is possible that in the future we may observe a young pulsar that is still in the unstable region. Furthermore, gravitational waves might even be detected from so far unknown young compact stars that have not been seen because their electromagnetic radiation is either too faint or it is absorbed or outshined by the supernova remnant. This possibility is interesting since there are several known young supernova remnants, including most notably SN 1987A, where a compact object has not been observed, yet. In view of the upcoming

next generation of gravitational wave detectors like advanced LIGO [11] it is therefore important to understand the expected gravitational radiation of such sources in detail.

Above we already gave semi-analytic expressions for two important quantities in this respect, namely the rotational angular velocity Ω_f (eq. (27)) when the star exits the r-mode instability region, which is related to the lower bound ν_f of the gravitational wave spectrum via $\nu = 2/(3\pi)\Omega$, and the spindown time t_{sd} (eq. (38)), which is the maximum age up to which gravitational waves from such a source could be observed. For a standard neutron star, using eq. (31), we estimate $\nu_f \approx (81.9 \pm 12.5) \text{ Hz } \alpha_{\text{sat}}^{-5/92}$. To have a reliable estimate for the lower bound of the spectrum is particularly important since advanced LIGO will have a significantly improved sensitivity below 100 Hz which coincides with the final stages of the r-mode spindown. Since the r-mode evolution becomes slow at low frequencies this region is where the evolution spends the most time and the analytic expression for the spindown time as a function of the dependent parameters should then allow us to estimate the probability that sources within the reach of advanced LIGO are currently active and observable.

A. Gravitational emission due to r-modes

In this section we follow and extend the previous analysis [10] and derive general results for the gravitational wave strain based on our analytic solution of the r-mode evolution. An explicit expression for the gravitational wave strain, averaged over polarizations and the orientation and position of a source at distance D on the sky, was given in [10, 52]

$$h = \sqrt{\frac{3}{80\pi}} \frac{\omega^2 S_{22}}{D}, \quad (41)$$

with the mass current quadrupole moment

$$S_{22} = \sqrt{2} \frac{32\pi}{15} GM\alpha\Omega R^3 \tilde{J}. \quad (42)$$

The strain depends both on the time-dependent r-mode amplitude and angular velocity

$$h(t) = \sqrt{\frac{2^{15}\pi}{3^5 5^3}} \frac{\tilde{J} GM R^3 \alpha(t) \Omega(t)^3}{D} \quad (43)$$

This expression has 3 different limits. Initially the amplitude rises exponentially whereas the frequency is fixed. Depending on the amplitude there can be an intermediate period where both α is saturated but Ω does not appreciably spin down yet, since the first term in eq. (36) dominates. Finally, at late times, when the second term

in eq. (36) dominates, the expression becomes independent of the initial conditions.

At saturation the r-mode amplitude can be replaced using the spindown equation (20). which gives

$$h(t) = \sqrt{\frac{9}{20} \frac{GI\dot{\Omega}(t)}{D^2\Omega(t)}} \quad (44)$$

This expression gives the strain in terms of the present frequency and the spindown rate. Assuming that r-modes dominate the spindown, this expression yields for sources with known timing data the standard *spindown limit*. This limit, which is analogously obtained e.g. for gravitational waves due to an ellipticity of the source, is very useful since it gives the maximum signal that can be expected for a given known source. There is only a chance to detect gravitational waves - or alternatively learn something about the source from a non-detection - if the detector sensitivity is lower than the spindown limit.

However, according to the discussion in section V the observed pulsars do not emit gravitational waves due to r-modes any more, and timing data is not available for other promising young sources, like compact objects in supernova remnants or pulsar spin nebulae. Only the age is usually roughly known. A prediction for the gravitational strain requires therefore an actual solution of the evolution. Previously a standard spindown equation with a general braking index [6] has been used to derive the strain as a function of the age of the source [53]. This expression also applies to the emission due to ellipticity and at late times it proved to be independent of the saturation amplitude. In the case of r-modes the strong heating generally requires a solution of the coupled set of evolution equations (20) and (21), though. As discussed in section IV the spindown evolution decouples only in the special case of a constant saturation amplitude. However, due to the r-mode heating the evolution predicted by this toy model can be quite different from that obtained from the coupled system for realistic saturation mechanisms, where the saturation amplitude is generally a function of temperature and frequency. Our analysis leading to the effective spindown evolution eq. (34) confirms that the study performed in [53] does indeed apply to r-mode gravitational wave emission. The effective braking index eq. (35) gives the explicit connection for a realistic r-mode saturation mechanism. Inserting the frequency evolution (eq. (36)) and the general form for the saturation amplitude (eq. (22)), there are significant cancellations and in the late time limit, where the frequency is far below the initial frequency, the strain becomes

$$h(t) \xrightarrow{\Omega \ll \Omega_i} \sqrt{\frac{3}{40} \frac{CGI}{D^2t}} \quad (45)$$

with the same constant \mathcal{C} describing the saturation mechanism (eq. (39)) that appeared before in the spindown

time. This expression agrees with the result in given in [47] using the effective braking index eq. (35). A striking property of eq. (45) is that it is indeed *independent* of the unknown saturation amplitude and even of the complete microphysics, including the cooling mechanism. Therefore, the strain of a given source is, up to moderate uncertainties in the moment of inertia (eq. (15)) and the constant factor \mathcal{C} involving β and γ , completely determined by its distance and its age. We recall that the constant \mathcal{C} is 1 for a constant saturation model ($\beta = \gamma = 0$), where the expression directly reduces to the result given in [47, 53], and somewhat larger for general saturation models. Because of the square root, the dependence on the saturation model is even weaker and the result does not change by more than some tens of per cent for realistic values $|\beta|, |\gamma| < 2$ predicted by different saturation mechanisms¹² [4, 23–25]. Therefore, the simple expression eq. (45) confirms and generalizes the result of [47, 53] to the more complicated case of r-mode emission with realistic saturation mechanisms, where the thermal heating significantly affects the spindown.

The analytic expression for the cutoff frequency eq. (27) also allows us to determine the final gravitational wave strain emitted in the last stage of the evolution $h_f \equiv h(\Omega_f)$ in terms of the final frequency Ω_f eq. (27). For a neutron star the final gravitational strain is

$$h_f^{(NS)} \approx 7.23 \cdot 10^{-27} \alpha_{\text{sat}}^{\frac{77}{92}} \left(\frac{\text{Mpc}}{D} \right). \quad (46)$$

The emitted gravitational wave strain during the evolution is shown in fig. 6 for different values of the saturation amplitude. The numerical curves are compared to the analytic results for the minimum gravitational strain, which is emitted at the end of the evolution eq. (46) and denoted by the points. As can be seen, small amplitude r-modes have a lower maximum amplitude but emit low amplitude gravitational waves over longer times. The plot shows that given the relevant age range of young pulsars, for saturation amplitudes $\alpha_{\text{sat}} \gtrsim 10^{-4}$ the late time approximation eq. (45) should be justified. For much smaller amplitudes the star is hardly spun down by r-modes, but in this case other spindown mechanisms, like magnetic dipole radiation, will dominate and determine the spindown $\Omega(t)$. This scenario, which is unlikely according to our results in section V, is discussed for completeness in appendix A.

¹² Although this is not the case for the saturation mechanisms cited, a general saturation mechanism, e.g. non-linear hydrodynamics effects [26, 27], could impose a more complicated function $\alpha_{\text{sat}}(\Omega, T)$. As argued before such a function is nevertheless approximated locally in different regions by the simple power law form eq. (22). The prefactor in eq. (45) would then be locally different, but because of the small size of the variation it would not change the conclusion.

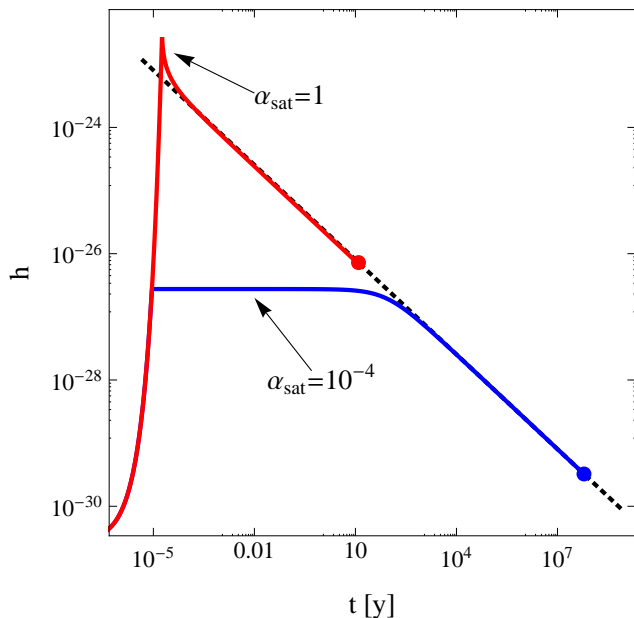


Figure 6: The time evolution of the gravitational wave strain of a $1.4 M_{\odot}$ APR neutron star, spinning initially with its Kepler frequency and located at a distance of 1 Mpc. We show the numerical curves for two different r-mode saturation amplitudes $\alpha_{\text{sat}} = 1$ (top) and $\alpha_{\text{sat}} = 10^{-4}$ (bottom). The dotted line denotes the asymptotic late time expression eq. (45). The dots denote the analytic result for the minimum strain amplitude of the gravitational radiation emitted at the end of the r-mode evolution and the endpoints for other amplitudes lie on the dotted line.

B. Signal detectability

The comparison of signals to the detector sensitivity is generally done in terms of the *intrinsic strain amplitude*¹³ h_0 which is in case of r-modes given by [47]

$$h_0 = \sqrt{\frac{8\pi}{5} \frac{\tilde{J}GMR^3 (2\pi\nu)^3 \alpha_{\text{sat}}}{D}} = \sqrt{\frac{25}{3}} h. \quad (47)$$

Using the general constraints on the moment of inertia eq. (13) and (15) and the range of different saturation models [4, 10, 23–25] yields for a constant saturation amplitude the remarkably definite result

$$h_0 \approx 2.3_{-0.8}^{+3.5} \times 10^{-27} \sqrt{\frac{1000 \text{ y}}{t}} \frac{1 \text{ Mpc}}{D}, \quad (48)$$

where the uncertainty limits are conservative and should, as discussed before, likely exceed the realistic range.

For an actual detection of gravitational waves a systematic search strategy is required which takes into account the periodicity of the signal. In particular, this requires a detailed model of the expected signal and its change over the observation interval in order to search for it in the data via a given statistical method, like e.g. matched filtering. Only for known isolated pulsars with precise timing data, like frequency and spindown rate, is such detailed knowledge of the phase-coherent signal available. Otherwise a huge parameter space for whole classes of models with different frequencies, spindown rates, ... has to be searched which greatly complicates the analysis¹⁴. Reducing the computational cost in such searches is crucial since a coherent search over time scales of order years for such an unconstrained system is still not manageable. Therefore, one important aim of our work is to narrow down the parameter space and to identify the most promising parameter regions for different sources.

Naturally, the likelihood of detecting a continuous signal in gravitational wave searches increases with the observation time. This is usually taken into account by giving the equivalent intrinsic strain amplitude that would be observed within a given search at 95% confidence level. For a coherent search the intrinsic strain amplitude is given by [54]

$$h_0^{95\%} = \Theta \sqrt{\frac{S_h(f)}{\Delta t}}. \quad (49)$$

It is a property of the particular search analysis and depends both on the power spectral density¹⁵ S_h of the detector noise and the observation time Δt . The equivalent intrinsic strain amplitude eq. (49) relies on matched filtering and requires knowledge of the detailed form and time evolution of the coherent signal. Since this might not always be available, the sensitivity obtained using this method is an optimistic estimate for other methods, where e.g. signals are combined incoherently. For observed isolated pulsars with known timing behavior the prefactor is $\Theta \approx 11.4$ and for known isolated sources without timing data, like Cas A or hypothetical localized compact sources within known supernova remnants, it is about 35 [53]. In the following we will discuss the detectability of gravitational waves in terms of the intrinsic strain amplitude, but other sensitivity measures have been used in the literature [10] and we will discuss some of them and their reliability in appendix B.

In fig. 7 our results for h_0 from gravitational wave emission by r-modes for different neutron star models are

¹³ This is the amplitude measured by a detector at one of the earth's poles of a source directly over it whose rotation axis is parallel to that of the earth.

¹⁴ This holds even more for sources in binaries, which we will not discuss here since the fraction of young pulsars in such systems is small.

¹⁵ The “power spectral density” is just the square of the amplitude spectral density of the noise expressed in equivalent gravitational wave strain, as given e.g. by the LIGO collaboration [55].

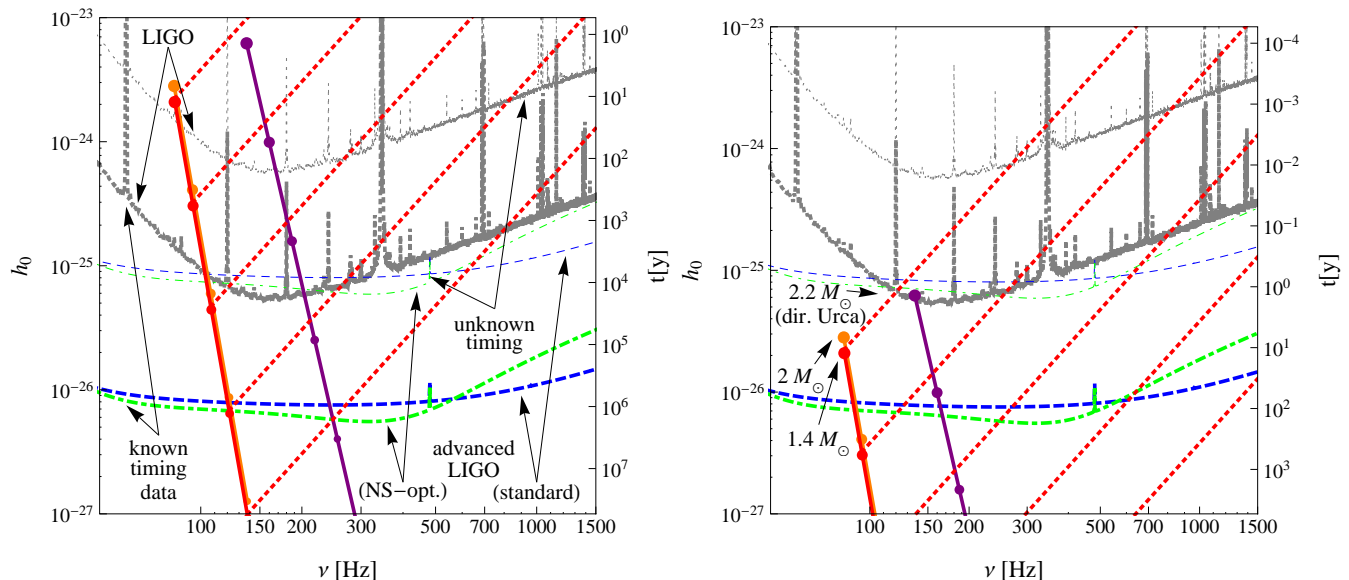


Figure 7: The frequency dependence of the intrinsic strain amplitude for different sources compared to the signal detectability of different detectors and for different observation periods. *Left*: Source within the galaxy (10 kpc), *right*: source within the local group (1 Mpc). The steeply decreasing solid lines show the minimum strain at the end of the r-mode evolution as a function of the gravitational wave frequency. These are shown for the three different APR stars given in tab. II. The dots show the strain for a few fixed values of the saturation amplitude of different orders of magnitude $\alpha_{\text{sat}} = 1$ (top) to $\alpha_{\text{sat}} = 10^{-4}$ (bottom), and the dotted curves ending at these points show for the $1.4 M_{\odot}$ star the evolution at earlier times. These curves are given for the constant r-mode saturation model which is a lower bound for the strain amplitude within other saturation mechanisms (see eq. (45)). The theoretical results are compared to the sensitivity of LIGO (solid) and the anticipated sensitivity of advanced LIGO [11] in the standard mode (dashed) and the neutron star optimized configuration (dot dashed). These are given both for a known pulsar search with one year of data (thick) and a search for potential sources without timing information using one month of data (thin). The right labels denote the age of the source assuming a constant saturation amplitude.

compared to the sensitivity curves¹⁶ for the LIGO detector (S6 run) and the projected advanced LIGO sensitivity [11], in both the standard (“ZERO_DET_high_P”) and the neutron star optimized mode (“NSNS_Opt”). For each detector, we show the two exemplary cases of a coherent search for known pulsars (where $\Theta = 11.4$) using one year of data (thick) and a search for sources without timing data, i.e. neutron stars or unseen compact remnants (using $\Theta = 35$) with an analysis of a month of coherent data (thin). The left panel assumes a typical source within the galaxy ($D = 10$ kpc) and the right panel a source in the local group of galaxies ($D = 1$ Mpc). The label on the right axis also shows the age of the object according to the direct relation for constant saturation amplitude eqs. (45) and (47). Let us first discuss this general relation. As can be seen LIGO could have detected r-mode emission from known galactic pulsars up to an age of about ten thousand years. According to our analysis in the preceding section, this should have been sufficient to see gravitational wave emission from all

such sources that can be seen, but unfortunately there are likely no known young pulsars that are currently in the r-mode phase. For known pulsars the sensitivity enhancement of advanced LIGO might therefore not help. But in case we detect in the future an even faster pulsar that is less than a hundred years old, then its r-mode emission could be detected with advanced LIGO even if it is extragalactic. There are a few such candidates including most notably SN 1987A in the Large Magellanic Cloud. For sources without timing data LIGO would have only seen galactic sources that are at most a few dozens of years old and only within a narrow frequency range. There has not been a galactic supernova for a long time and therefore it is not surprising that LIGO did not make a detection. In contrast advanced LIGO could, thanks to its flat noise spectrum, detect a galactic source over the entire relevant frequency range and up to an age of more than a thousand years. As discussed before, this is exactly the age range favored by the r-mode scenario for the spindown of the observed pulsars and therefore advanced LIGO is a very promising machine for the detection of gravitational waves from r-mode oscillations of young neutron stars. Moreover, for extragalactic supernovae the sensitivity of advanced LIGO should be sufficient to see r-mode oscillations of a compact remnant in the immediate aftermath up to about a year. For sources as far as the Virgo cluster

¹⁶ The sensitivity curves have been released by the LIGO scientific collaboration and were obtained from <http://www.ligo.org/science/data-releases.php> and as technical document T0900288 at <http://dcc.ligo.org>.

of galaxies, as originally discussed in [10], even with advanced LIGO a detection should only be possible under extremely lucky circumstances and third-generation detectors like the Einstein telescope [56] will be necessary to take advantage of the much larger number of more distant sources.

Next consider our theoretical results in fig. 7, which are given for the different neutron stars listed in table II. Namely the $1.4 M_{\odot}$ and $2 M_{\odot}$ APR stars for which only modified Urca reactions are possible and the $2.2 M_{\odot}$ star where direct Urca reactions are present within its core. The steeply descending solid lines show the minimal signal emitted at the end of the r-mode spindown evolution (where the star spends most of its time) as a function of the frequency, which in turn is a function of the unknown saturation amplitude. The dots show the result for fixed saturation amplitudes of different orders of magnitude ranging from $\alpha_{\text{sat}} = 1$ (top) to $\alpha_{\text{sat}} = 10^{-4}$ (bottom). The dotted curves show the r-mode evolution for the $1.4 M_{\odot}$ model for these saturation amplitudes. As expected the signal is larger and emitted at higher frequencies if the star is younger but a star also spends far less time in these earlier stages. Although a star of a given age emits gravitational waves with a fixed strain amplitude, depending on the unknown saturation amplitude the frequency of these gravitational waves can be very different. As suggested by the analytic results, the strain depends little on the mass and the details of the composition, and the size of (suppressed) error bands on these curves would be given by the errors in prefactor of eq. (48). This insensitivity holds even for the case of the heavy star where direct Urca emission is possible. As noted before, because of the much stronger cooling in this case the star spins down at a lower temperature where the boundary of the instability region is at a larger frequency, so that the lower gravitational wave cutoff frequency is considerably higher. Yet, up to this point the gravitational wave signal is nearly identical to the standard case with modified Urca cooling. This is an important observation since the data on Cas A [57], which is the only young star for which the cooling has been explicitly observed, clearly points to an enhanced neutrino emission mechanism. The standard explanation [58, 59] is emission due to pair breaking of superfluid neutrons which is in between the cases of modified and direct Urca emission discussed here.

C. Searches for promising sources

The fact that nearly all known pulsars spin too slowly to emit gravitational waves due to r-modes at the moment requires us to consider other potential sources. Here we give the expected signal for a few examples of known possible sources that could be young enough to emit gravitational waves due to r-modes. These consist of, in addition to the fastest pulsar J0537-6910 discussed above, the young neutron star Cassiopeia A from which no pulsation

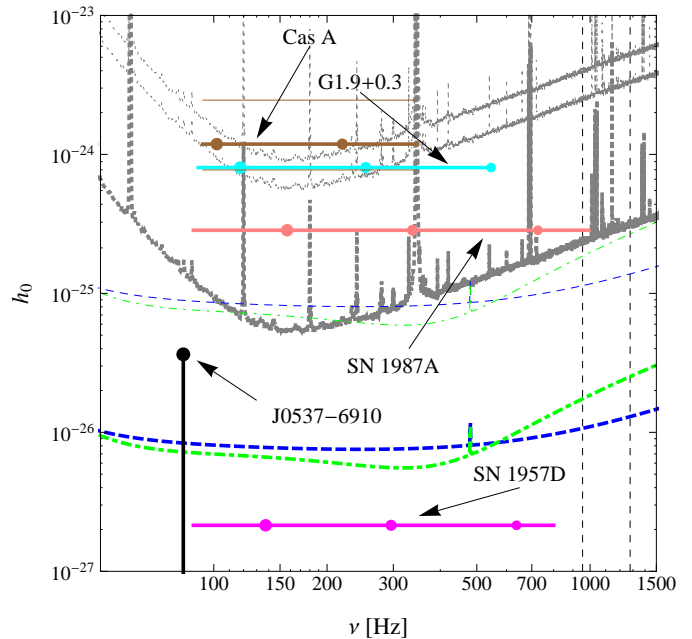


Figure 8: The frequency dependence of the intrinsic strain amplitude for potential realistic sources. The actual age of these sources as well as their distance have been used and the expected frequency range determined from these known parameters is shown. The frequency range corresponds to a range of saturation amplitudes and the dots denote the corresponding values for different orders of magnitude from $\alpha_{\text{sat}} = 0.1$ to 10^{-3} . We also included the fastest young pulsar J0537-6910 for which the observed frequency is used and where the dot represents the result if r-mode spindown dominates and lower values are possible if other spindown sources are important. The detector curves are the same as in fig. 7 with the addition of the uppermost curve which shows the sensitivity of a previous Cas A search [62]. The two thin vertical lines show for comparison the corresponding frequency of the fastest observed (old) pulsar and that corresponding to the maximum Kepler frequency of the star.

has been observed [60] and several supernova remnants where no compact object has been detected so far. However, it has recently been suggested that the hard X-ray emission from SN 1957D results from a pulsar wind nebula and the compact remnant which produced it would then be the youngest indirectly observed pulsar [61]. We take into account both the age and the available distance estimate for these sources shown in tab. IV. As noted before, the strain amplitude is fixed by these parameters, but the frequency can vary depending on the unknown r-mode saturation amplitude.

Because of the significant computational cost of a gravitational search it is essential to know the spindown model and the expected timing parameter range for a given source [53, 55]. In gravitational wave searches the expected signal is usually modeled by a generic spindown model [6]

$$\dot{f} \sim -f^n \quad \Rightarrow \quad \ddot{f} = n\dot{f}^2/f \quad (50)$$

with a fixed braking index n . Since the spindown evolution is coupled to the thermal evolution in the case of r-mode emission, up to now it might have seemed questionable whether the simple model eq. (50) is appropriate. However, our general analysis in section IV showed that the thermal evolution is always faster than the spindown (eq. (24)) and can be solved in a first step. Therefore the effective spindown equation (34) takes indeed the standard form eq. (50), yet with an effective r-mode braking index n_{rm} given in eq. (35). As discussed, the saturation model can change the braking index from the canonical value 7 to significantly smaller values. E.g. for mode coupling with damping due to shear viscosity [25] the braking index is considerably reduced to $n_{rm}^{(mc)} = 4$. This is important both for the search for gravitational waves, as well as for the interpretation of the results in case a detection is made. Generally, a hierarchy of braking indices was expected, namely 3 for electromagnetic dipole emission, 5 for gravitational waves from an ellipticity of the star (or electromagnetic quadrupole emission) and 7 for r-mode emission¹⁷. Our results show that analogous to electromagnetic emission, where the observed braking indices are below 3, the possible braking indices due to r-modes are likewise systematically lower and the uncertainty in the unknown saturation mechanism is even larger - to the point where even a discrimination between electromagnetic and gravitational wave spindown becomes questionable. Therefore it should be hard to determine the spindown mechanism from current electromagnetic pulsar timing data. However, future gravitational wave observations could change this. Comprehensive information on the source, the gravitational wave amplitude and the timing data, could due to the distinct r-mode braking indices eq. (35) and the quantitative prediction of the r-mode signal eq. (45) eventually even allow us to determine the r-mode saturation mechanism observationally.

As discussed before, the lower boundary of the frequency range of the expected gravitational wave signal is rather insensitive to the details of the source and set by where the r-mode evolution exits the instability region, see fig. 2. The corresponding α_{sat} can be obtained by equating eq. (38) to the known age of the source which then determines the final frequency. In contrast, the upper boundary is not restricted by gravitational wave emission alone because the r-mode amplitude could in principle be arbitrary small. Yet, in this case other spindown mechanisms will dominate and set a limit on the frequency to which a potential pulsar would have been spun down at the age of a considered source. To estimate

this effect, we assume again the spindown model eq. (50) with a fixed braking index n . The proportionality constant is related to the characteristic age $t_c \equiv -\left(f/\dot{f}\right)_0$ of a given pulsar and the evolution is then given by

$$f(t) \approx \left(\frac{1}{f_i^{n-1}} + \frac{(n-1)t}{t_c f_0^{n-1}} \right)^{-\frac{1}{n-1}}. \quad (51)$$

For a conservative estimate of the upper limit we assume a braking index of $n = 2.5$ and choose the initial frequency f_i as the Kepler frequency of our $1.4 M_\odot$ model. Fiducially choosing the population of young stars as those in the ATNF database with spindown rate $\dot{f} > 10^{-11} \text{s}^{-2}$, the largest value for $t_c f_0^{n-1}$ is, as could have been expected, obtained for J0537-6910. Let us assume that the observed population of pulsars is characteristic for the spindown behavior of so far unobserved sources. This then allows us to estimate an upper limit for the frequency to which other spindown mechanisms would have spun down a (potentially unobserved) compact star in a considered source even when gravitational wave emission would be negligible for the spindown. Finally, consider pulsars with known timing solution, where both the frequency and the spindown rate are known. If r-mode emission dominates the current spindown, eq. (20) determines the saturation amplitude (see fig. 5) and in the case of J0537-6910 we find $\alpha_{\text{sat}} \approx 0.084$. If other spindown mechanisms are important as well, α_{sat} and the resulting gravitational strain would be lower.

Our results are shown in fig. 8. Again the sources without known timing data should be compared to the thin curves, whereas the expected strain for the pulsar J0537-6910 should be compared to the thick curves. As can be seen there should be a realistic chance to see Cassiopeia A, and potentially a compact remnant in the youngest known galactic supernova G1.9+0.3, from a coherent analysis of a month of LIGO S6 data. Even more strikingly the frequency range where Cas A is above the detector sensitivity coincides with the expected frequency range for this source. For Cas A a detailed previous LIGO analysis failed to detect a signal, but imposed strict bounds on a potential r-mode amplitude of this source [62]. Yet, this was done with only 12 days of S5 data. As can be seen by the uppermost thin detector curve in fig. 8, which shows the S5 sensitivity for this shorter observation interval, we find that the signal is just at the detection limit and even this only over a narrow frequency range, so that it is not too surprising that no detection was made. Cas A should therefore be a prime target for advanced LIGO and according to our results it should even be promising to perform another search of the S6 data if a coherent analysis of a whole month of data is computationally feasible. The signal of 1987A is about an order of magnitude smaller, but it would be in the reach of advanced LIGO which could detect it over the entire expected frequency range (which is larger due to its young age). The youngest candidate

¹⁷ If several mechanisms are relevant intermediate values are possible [6].

pulsar, produced by SN 1957D, would be an ideal target, but it is unfortunately too distant to detect gravitational waves due to r-mode emission with advanced LIGO and more sensitive future detectors will be required. Our results show that as soon as the pulsar is directly detected and timing data becomes available this source should be in the range of the forthcoming Einstein telescope [56], which has an order of magnitude higher sensitivity compared to advanced LIGO. If against all odds the fastest directly observed young pulsar J0537-6910 is still in the final stage of its r-mode evolution there is a good chance that its signal, which was below the threshold of the original LIGO detector, will be detected by advanced LIGO.

The relevant ranges for the timing parameters, given in table IV, should help to perform future searches. If r-mode emission dominates the spindown, the frequency and spindown rate are related by eq. (20) and the time variation over the observation interval is given by the semi-analytic solution eq. (36). In reality where other spindown mechanisms are present as well there should nevertheless be a strong correlation between frequency and spindown rate so that it is not necessary to search the complete range in frequency and spindown rate but a (narrow) parameter region around the ideal r-mode spindown behavior should be sufficient. This could strongly reduce the required parameter range in dedicated r-mode search. In case of Cas A the frequency range obtained here by our dynamical analysis roughly agrees with the previously used fiducial range $100 \text{ Hz} \leq \nu \leq 300 \text{ Hz}$ chosen by sensitivity arguments [62]. Finally it is important to note that the saturation amplitudes corresponding to the above relevant gravitational frequency ranges, as denoted by the dots in fig. 8, are precisely in the range $10^{-2} \lesssim \alpha_{\text{sat}} \lesssim 10^{-1}$ which is required for an explanation of the low frequencies of observed young pulsars within the r-mode scenario discussed in section V. This should provide an incentive to search for gravitational wave emission from r-modes of sufficiently young compact sources.

VII. CONCLUSIONS

We have derived general semi-analytic results for the r-mode spindown evolution eqs. (36) and (37) of young pulsars that completely reveal the dependence on the relevant physical ingredients. We find that the key quantities like the final spin frequency eq. (27) are remarkably insensitive to the microphysical material properties. For macroscopic input quantities like the moment of inertia of the star or the angular momentum of the mode we gave rigorous bounds that allow us to estimate the uncertainty in these parameters. We show that the thermal evolution is always faster than the spindown evolution. Therefore, if the form of the instability region is convex, a steady state is reached where viscous heating equals cooling due to neutrino emission. Non-convexity of the instability region due to stability windows arising from

enhanced dissipation due to exotic phases of matter can prevent the star from reaching the thermal steady state and thereby drastically change the evolution which could lead to clear astrophysical signatures [36].

The semi-analytic results for the final frequency of the evolution enabled a quantitative comparison to pulsar timing data and we find that all stars except one lie clearly below the frequency to which r-modes can spin down a young pulsar. Only the fastest spinning young star PSR J0537-6910 is fast enough that it could lie within the instability region. Using additional observations of spindown rates we find that this is unlikely since it lies just at the lower border of the uncertainty range. The spindown time in contrast depends strongly on the saturation amplitude and increases quickly from time scales of order years at $\alpha_{\text{sat}} \approx 1$ to more than a million years below $\alpha_{\text{sat}} < 10^{-3}$.

The r-mode scenario can therefore provide a quantitative explanation of the low spin frequencies of young pulsars if the saturation amplitude is within certain limits. On the one hand it has to be sufficiently large $\alpha_{\text{sat}} \gtrsim 0.01$ for the spindown to be fast enough to dominate other possible spindown mechanisms and result in spindown times less than a few hundred years, which is shorter than the age of observed pulsars. On the other hand, even taking into account the significant uncertainties, a very large saturation amplitude $\alpha_{\text{sat}} \approx 1$ would have spun PSR J0537-6910 down to its current frequency in less than a hundred years. This would be in clear conflict with the much larger age estimate of its remnant of roughly 5000 years [48] and the significant present spindown rate of the pulsar, which is most likely due to electromagnetic radiation and should have further sped up the spindown. Different saturation scenarios - which are here studied in a generic way via a function $\alpha_{\text{sat}}(\Omega, T)$ - do not significantly change the spindown time and therefore should not qualitatively affect our bounds on the saturation amplitude. In case r-modes reach sizable amplitudes $0.01 \lesssim \alpha_{\text{sat}} \lesssim 0.1$, PSR J0537-6910 could be younger than its characteristic age - obtained within a pure magnetic dipole model - suggests. If in contrast r-modes saturate already at amplitudes $\alpha_{\text{sat}} \ll 0.01$ they would be subleading compared to the other spindown mechanisms, which must be sizable according to the significant spindown rates of observed young pulsars.

Since we find that probably no observed pulsar is at present spinning down due to r-modes, one has to be careful when interpreting spindown limits on r-mode amplitudes from young stars [47]. Although these limits give important information on these stars, they are trivially fulfilled if the r-mode has already decayed. In this case the current rate involves only information on other spindown mechanisms, like magnetic dipole emission, and cannot give a bound on the r-mode saturation amplitude during the era when r-modes were actually present. The spindown limit [47] simply extrapolates the solid lines in fig. 5 outside the instability region. In reality for a large saturation amplitude the star would actually spin down

source	age [y]	D [kpc]	ν [Hz]	$\dot{\nu}$ [10^{-9} s^{-2}]	h_0	h_c	$\frac{S}{N} _{\text{LIGO}}^{(obs)}$	$\frac{S}{N} _{\text{aLIGO}}^{(obs)}$	$\frac{S}{N} _{\text{aLIGO}}^{(tot)}$
J0537-6910	?	52	83	-0.27	3.6×10^{-26}	$6.5 (6.8) \times 10^{-20}$	2.1 (0.2)	28 (2.8)	—
SN 1987A	25	51.5	[84, 992]	[-18, -265]	2.8×10^{-25}	$0.8 (1.2) \times 10^{-19}$	23 (18)	221 (236)	$2.0 (3.2) \times 10^3$
SN 1957D	55	4610	[86, 801]	[-8.3, -155]	2.1×10^{-27}	$0.9 (1.3) \times 10^{-21}$	0.2 (0.1)	1.6 (1.8)	19 (33)
G1.9+0.3	≈ 140	7.7	[89, 545]	[-3.3, -59]	8.0×10^{-25}	$4.9 (7.2) \times 10^{-19}$	57 (62)	598 (662)	$0.9 (1.8) \times 10^4$
Cassiopeia A	≈ 300	3.4	[91, 346]	[-1.5, -19]	1.2×10^{-24}	$1.0 (1.5) \times 10^{-18}$	83 (106)	906 (1015)	$1.3 (3.7) \times 10^4$

Table IV: Expected gravitational wave signal and expected range of the timing parameters for different young sources in case there is an associated fast rotating compact object that spins down via the r-mode mechanism. The alternative sensitivity measures in the right part of the table are discussed in detail in appendix B and they generally strongly overestimate the detectability since they do not take into account our limited knowledge of the source or not even the limited observation time. All values are given for a $1.4 M_{\odot}$ APR star with $\alpha_{\text{sat}} = 0.1$ (0.01); for $\alpha_{\text{sat}} = 1$ r-modes would have already decayed at the current age of these systems. The observable signal-to-noise ratios are computed assuming an observation time $\Delta t = 1$ y. The theoretical total signal-to-noise ratios are here obtained by taking into account the total frequency interval $[\nu_f, \bar{\nu}]$ that is observable from the stars current age to the end of the r-mode spindown.

quickly inside but then the spindown rate would drop to a lower value determined by the other mechanisms once the star leaves the instability region. The slope of the curves for other spindown mechanisms are generally smaller, as illustrated in fig. 5 for the Crab and the Vela pulsar where a reliable braking index is available. An initial r-mode spindown can therefore be perfectly consistent with observations even for a large saturation amplitude as long as the star is currently already sufficiently far away from the instability boundary. Yet, in case of J0537-6910 which is still close to the instability boundary, the spindown limit is more restrictive and coincides with the limits given in the previous paragraph [47].

We considered in this work only the dominant $m = 2$ r-mode. The inclusion of higher multipoles might slightly affect the spindown time by a factor $\lesssim 1$ but will not change the final frequency since the corresponding instability regions of these modes are smaller [3] and therefore the final segment of the steady-state curve, where the evolution spends by far the longest time, is identical. Furthermore, we have here mainly studied the simplest case of a neutron star with damping due to leptonic interactions and modified Urca processes in the core. The main reason for this is that it is the case of minimal damping whereas other phases of matter or structural inhomogeneities will increase the damping [3, 30, 31, 34]. Therefore, the final spindown frequencies we find are the lower limit to which general compact stars can be spun down by r-modes. In reality several aspects like pairing, mutual friction, the crust and other spindown mechanisms complicate the analysis. Although we did not study these in detail here, our general semi-analytic expressions allow us to study any single source of damping, such as the effect of an Ekman layer.

Nuclear pairing could strongly change the temperature dependence of material properties over the considered temperature regime so that it would not have a simple power law form. Therefore it should alter thermal evolution, but since at saturation the thermal evolution does hardly affect the spindown (aside from the fact that its final frequency at the boundary of the instability region de-

pends on temperature) the results presented here should not be strongly affected by pairing. The relevant part of the boundary is determined by shear viscosity which is dominated by electromagnetic leptonic processes which are only indirectly affected by the presence of hadronic matter. As found in [32] this is a moderate effect and taking into account the insensitivity of our results to the shear viscosity this should only slightly increase the considered error range.

As discussed before mutual friction in superfluid systems is an additional source of damping that could considerably shrink the instability region. If this effect is very strong it could significantly raise the frequency to which r-modes can spin down a star. As can be seen from fig. 2 if the enhanced damping is only present at low temperatures, e.g. $T < 10^9$ K as assumed in [10], this would affect the evolution strongly at low saturation amplitudes but only moderately at sufficiently large amplitudes favored above.

Furthermore, it has been argued that the boundary layer at the interface between the core and the crust strongly enhances the viscous damping which would reduce the r-mode instability region [63]. This mechanism is based on the picture that there is a sharp boundary and the fluid velocity drops to zero over a distance of a few centimeters. However, in reality the crust is a complicated structure with possible geometrically structured pasta phases and an inner crust where the concentration of the neutron fluid decreases continuously. The transition from a pure fluid to a rigid lattice then happens gradually over a large distance and it is questionable why the above picture should apply here. Phenomenologically these effects have partly been modeled via a slippage parameter and the impact becomes rather small for likely parameter values [31]. We note, however, that our general analytic expressions should also apply when the crust provides the dominant source of dissipation, as encoded in the values of the general parameters in table I. In this case further complications like the breaking or melting of the crust could be relevant which in turn should reduce the effect of viscous boundary layer damping.

Finally, we computed the gravitational wave emission due to the r-mode spindown of young stars. We compare our results in terms of the intrinsic strain amplitude to the sensitivity of the LIGO and advanced LIGO detector for realistic searches for sources with and without timing solution. This properly takes into account the finite observation interval of such searches which had been neglected in initial r-mode analyses [10]. We point out the remarkable property that the intrinsic strain amplitude is *independent* of the saturation amplitude and almost independent of the saturation model which only enters via a constant factor close to one. Therefore, the gravitational wave signal depends effectively only on the age of the source and its distance. The reason for this independence is that the emitted gravitational wave signal increases both with the r-mode amplitude and the frequency. A star of a given age will still be spinning quickly if the saturation amplitude is low, but will have spun down to a low frequency if the saturation amplitude is high. These competing effects cancel each other. For realistic observation intervals, we find that LIGO could have seen young sources in the galaxy (distance 10 kpc) with known timing solution up to an age of about 10^4 years, whereas sources without timing solution that are older than a few tens of years would have been undetectable. Advanced LIGO in contrast should increase both of these age ranges by about a factor of a hundred. Since according to our analysis none of the observed pulsars is likely to be in the r-mode phase, very young sources without a timing solution should be promising targets for gravitational wave searches, and advanced LIGO should be able to detect them over the entire relevant age range of up to thousands of years. For more distant sources in the local group of galaxies (distance 1 Mpc) these ages are reduced by a factor of ten thousand so that in this case probably only sources with a known timing solution are detectable. We also considered a few explicit examples and find that Cas A, J0537-6910, and potential compact remnants in SN1987A and G1.9+0.3 are very promising targets that are within the sensitivity range of advanced LIGO. To restrict the computational cost of future searches we also provided estimates for the relevant search ranges of the unknown timing parameters of these sources.

The quantitative r-mode spindown scenario discussed here provides strong evidence that young pulsars could indeed emit observable gravitational wave signals. Both the steadily growing list of known young pulsars and the strongly increased sensitivity of second generation gravitational wave detectors make it a realistic possibility to detect gravitational radiation from r-mode oscillations in the near future. Future third generation gravitational wave detectors like the currently planned Einstein telescope [56] should then allow us to see many more potential sources at larger distances. This would mark the advent of gravitational wave astronomy as a way to learn about the internal composition of compact stars.

Appendix A: Very low saturation amplitude scenario

The quantitative explanation of the low spin frequencies of observed young pulsars discussed in section V points to a large saturation amplitude $\alpha_{\text{sat}} > 10^{-4}$. In this case the expected gravitational signal is large, independent of the saturation amplitude and even mostly of the saturation mechanism. However, one cannot completely exclude that the striking explanation of the pulsar spin data is a mere coincidence and the saturation amplitude is much smaller. For completeness we therefore discuss here this (unlikely) alternative scenario. Rather small saturation amplitudes are predicted by mode coupling models [23–25], whereas other mechanisms like non-linear hydrodynamic effects or suprathreshold viscosity lead to large saturation amplitudes. In case the amplitude is very small r-modes are irrelevant for the spindown since other spindown mechanisms like magnetic dipole emission dominate. The spindown evolution is then independent of the saturation amplitude. Using the generic parametrization eq. (50) with a braking index n the spindown is given by eq. (51). Nevertheless these low amplitude r-modes would emit gravitational waves. The gravitational wave strain is then given by eq. (43), where the frequency evolution is determined by the appropriate alternative spindown mechanism. For a standard neutron star spinning with frequency f we find in case of a small saturation amplitude

$$h_0 \approx 9.0 \times 10^{-26} \alpha_{\text{sat}} \left(\frac{f}{100 \text{ Hz}} \right) \left(\frac{1 \text{ Mpc}}{D} \right)$$

In this case the strain is proportional to the saturation amplitude since the spindown evolution is independent of the r-mode emission and there is no cancellation analogous to eq. (45). Therefore the strain is, according to our assumption that α_{sat} is small, strongly suppressed. We see that at an amplitude $\alpha_{\text{sat}} \approx 10^{-4}$ there is only a chance to detect the gravitational waves with advanced LIGO if the source spins fast and is very close. At even lower amplitudes $\alpha_{\text{sat}} \ll 10^{-4}$ a source would be undetectable.

Appendix B: Alternative sensitivity measures

For the analysis of the gravitational wave emission due to r-modes a variety of measures to compare to detector sensitivities have been used. For comparison with other work we discuss these in the following.

1. Power spectrum

An alternative way to discuss r-mode emission is via the Fourier spectrum. In principle this is interesting for periodic sources like neutron stars since the frequency

hardly changes over the short observation interval. The Fourier-transformed gravitational wave strain $\tilde{h}(\nu)$ in the frequency domain can be obtained in a stationary phase approximation as

$$\left|\tilde{h}(\nu)\right|^2 = |h(t)|^2 \left|\frac{dt}{d\nu}\right|. \quad (\text{B1})$$

As seen from fig. 6, there are two qualitatively different stages of the gravitational wave emission. The first arises from the growth phase of the r-mode and results in narrow spike in $\tilde{h}(\nu)$ at the star's initial frequency. This phase lasts only for a short time of order minutes and as shown in [10] there is not enough energy in this pulse to be detectable. Therefore, we neglect this initial part of the spectrum here. In the subsequent saturated phase where the star spins down it emits gravitational waves over a continuous frequency range with strain density

$$\tilde{h}(\nu) = \sqrt{\frac{9\tilde{I}GM R^2}{20D^2\nu}}. \quad (\text{B2})$$

The quantity that is usually used for a comparison with the detector sensitivity is the characteristic amplitude of the signal defined by $h_c \equiv \nu \tilde{h}$. In particular the minimum characteristic amplitude $h_{c,f} \equiv h_c(\nu_f)$ reached at the lower frequency boundary of the evolution is interesting. The square root in eq. (B2) makes the dependence of $h_{c,f}$ on the microscopic parameters even weaker than for the final frequency eq. (30). However, the expression depends more strongly on macroscopic quantities like the mass and the moment of inertia encoded in the parameter \tilde{I} . The rigorous bounds eq. (13) show that this dependence is also moderate since all these quantities vary only within roughly a factor of two. For a standard neutron star we find

$$h_{c,f}^{(NS)} \approx 1.6 \cdot 10^{-22} \left(\frac{\tilde{S}}{\tilde{S}_{\text{fid}}}\right)^{3/46} \left(\frac{\tilde{L}}{\tilde{L}_{\text{fid}}}\right)^{5/368} \left(\frac{\tilde{J}}{\tilde{J}_{\text{fid}}}\right)^{-29/184} \\ \times \left(\frac{\tilde{I}}{\tilde{I}_{\text{fid}}}\right)^{1/2} \left(\frac{M}{1.4 M_\odot}\right)^{63/184} \left(\frac{R}{11.5 \text{ km}}\right)^{281/368} \left(\frac{\text{Mpc}}{D}\right)^{-5/184} \alpha_{\text{sat}}. \quad (\text{B3})$$

Note that this quantity is also nearly independent of the saturation amplitude α_{sat} (and even increases with decreasing amplitude). The same holds for the microscopic parameters. For example the dependence on the neutrino emissivity involves the power 5/368 which provides a striking example of how insensitive such macroscopic observables can be to microscopically decisive yet inherently poorly known quantities, since even a drastic change by three orders of magnitude would only have an irrelevant effect of less than 10%.

The detector sensitivity is described by the rms strain noise $h_{\text{rms}} \equiv \sqrt{\nu S_h(\nu)}$ in terms of the power spectral density S_h of the detector noise. In contrast to eq. (49) this

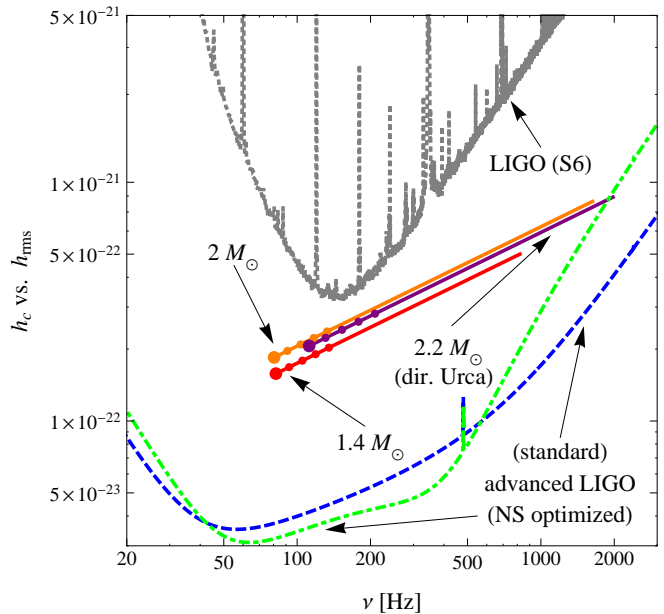


Figure 9: The characteristic gravitational wave amplitude of neutron stars, located somewhere in the Virgo cluster (distance 20 Mpc) and based on the different APR stars given in tab. II, compared to the sensitivity of the LIGO (dotted) and advanced LIGO (dashed) [11] detectors. The large dots denote the analytic expressions for the lower frequency limit for an amplitude $\alpha_{\text{sat}} = 1$ and the smaller ones for lower amplitudes down to $\alpha_{\text{sat}} = 10^{-4}$.

quantity is only a measure of the general sensitivity of the detector but not of a particular search and contains neither information on the source nor on the observation interval. In order for the characteristic amplitude to give a meaningful estimate the observation time should be comparable to the time scale of the frequency change of the signal (so that all strength of a given frequency is actually detected). Clearly for small saturation amplitudes where the spindown time increases drastically with decreasing α_{sat} , see eq. (40) and table III, this is not guaranteed and therefore the fact that the characteristic amplitude is above the background alone is not sufficient for a detection.

The result for the characteristic amplitude in the saturated regime is given for different stars in fig. 9. Whereas the spectra of the two standard neutron stars with modified Urca reactions have nearly the same lower frequency cutoff, the heavy star with direct Urca interactions in the core has a higher cutoff > 100 Hz, but otherwise features a characteristic amplitude of similar size, as could have been expected from the insensitivity to the neutrino emissivity in eq. (27).

2. Theoretical signal detectability

In [10] the following expression for the signal to noise ratio for matched filtering was given

$$\left(\frac{S}{N}\right)^2 \Big|^{(\text{tot.})} = 2 \int_{\nu_{\min}}^{\nu_{\max}} \frac{d\nu}{\nu} \left(\frac{h_c}{h_{\text{rms}}}\right)^2 = \frac{9I}{10D^2} \int_{\nu_{\min}}^{\nu_{\max}} \frac{d\nu}{\nu S_h(\nu)} \quad (\text{B4})$$

in terms of the power spectral density S_h of the noise and ranging over a range from the final frequency of the r-mode evolution $\nu_{\min} = \nu_f$ to the initial frequency $\nu_{\max} = \nu_i$ at which the star is created. Here the label (tot.) has been added to indicate that the total frequency spectrum is included in this quantity. This point will be discussed in more detail below. In eq. (B4) logarithmic frequency intervals are weighted by $1/S_h$, since at low frequencies the frequency changes slowly which makes it easier to detect the periodic signal. After a numerical integration an approximate fit to the result over the relevant parameter ranges for ν_{\min} and ν_{\max} is given for the advanced LIGO detector by¹⁸

$$\frac{S}{N} \Big|_{\text{aLIGO}}^{(\text{tot.})} \approx 4.09 \cdot 10^{23} \sqrt{\text{Hz}} \frac{\sqrt{GI}}{D} \times \sqrt{1 + 0.40 \log\left(\frac{\nu_{\max}}{1000 \text{ Hz}}\right) + 0.36 \frac{100 \text{ Hz} - \nu_{\min}}{100 \text{ Hz}}}. \quad (\text{B5})$$

Compared to the result given in [47] for the anticipated second generation LIGO detector we find a much weaker dependence on the minimum final frequency and a stronger dependence on the unknown maximum initial frequency. By inserting the result for the minimum frequency eq. (30) we see that the uncertainty of this result due to the microphysics is minor. The main uncertainty arises from the moment of inertia which using the above bounds has a maximum theoretical uncertainty given in eq. (15).

The signal to noise ratios for different sources at different distances are shown in table V. Here we compare the values for sources given by the different considered stars listed in tab. II. These are assumed to be located at different distances, namely in the Virgo Cluster (20 Mpc), the Local group of galaxies (1 Mpc) and within the Milky way (30 kpc). Using the actual anticipated noise background of the advanced LIGO detector and without the assumption that the evolution stops at 10^9 K,

¹⁸ We fit the integrated form rather than the initial strain noise S_h , since this provides a more precise result. Fitting the strain noise with a double power law $S_h(\nu) \approx a\nu^{-2} + b\nu^2 + c$, similar to the ansatz used in [47] before their subsequent approximation, we can perform the integration analytically, yielding the same qualitative leading parameter dependence on ν_{\min} (power law) and ν_{\max} (logarithmic) we use for the fit in eq. (B5).

our values are slightly larger than those obtained in [10]. Heavier stars tend to give larger values due to the larger moment of inertia whereas direct Urca processes reduce the signal to noise ratio since the thermal steady-state curve is at lower temperatures and its intersection with the boundary of the instability region is correspondingly at a higher frequency that sets the lower gravitational wave frequency cutoff in eq. (B5). Yet, overall these values are rather similar for the different considered stars. These considerations suggest that theoretically a detection is possible for sources up to large distances in case the gravitational wave signal could be detected over its complete frequency range. However, this is inherently impossible for a continuous r-mode signal.

3. Practical signal detectability

The above total signal to noise ratios do not reflect the detectability of the signal of a given single source over the actual observation period, as noted already in [10]. They would provide such an actual measure for the detectability only for a short multi-wavelength signal that is completely observed, for example a binary inspiral. However, these ratios cannot give a reasonable measure in the present case where the source is monochromatic and changes slowly with time while it is only observed for a short time interval, since the frequency ranges in eq. (B4) that would only be detectable hundreds of years before or after the present observation can hardly affect the detectability within the limited observation interval. Therefore a proper signal to noise ratio that measures the detectability must take into account the finite duration of the observation and only include the relevant frequencies in eq. (B4).

To find a more realistic signal to noise ratio for the detectability in gravitational wave detectors, assume that the frequency of the source changes only slightly during the short observation time interval Δt over which it has an average frequency $\bar{\nu}$. The change $\Delta\nu \ll \bar{\nu}$ during this time interval can be obtained from eq. (20)

$$\Delta\nu \approx \frac{2}{3\pi} \frac{d\Omega}{dt} \Delta t = \frac{2\bar{\nu}Q\alpha_{\text{sat}}^2}{\tau_G(\bar{\Omega})} \Delta t. \quad (\text{B6})$$

The current angular velocity $\bar{\Omega}$ can be obtained in terms of the current age t of the star from the solution of the spindown equation eq. (20) which yields in the limit $\Omega_i \gg \bar{\Omega}$

$$\Delta\nu \approx -\frac{\bar{\nu}}{6} \frac{\Delta t}{t}. \quad (\text{B7})$$

For $\Delta\nu \ll \bar{\nu}$ the integral in eq. (B4) gives an estimate for the actual *observable* signal to noise ratio

neutron star	T_f [K]	f_f [Hz]	ν_f [Hz]	t_{sd} [y]	h_f @ 1 Mpc	$h_{c,f}$ @ 1 Mpc	$\frac{S}{N} _{\text{Virgo}}^{(tot)}$	$\frac{S}{N} _{\text{L.g.}}^{(tot)}$	$\frac{S}{N} _{\text{M.w.}}^{(tot)}$	$\frac{S}{N} _{\text{Virgo}}^{(obs)}$	$\frac{S}{N} _{\text{L.g.}}^{(obs)}$	$\frac{S}{N} _{\text{M.w.}}^{(obs)}$
APR $1.4 M_\odot$	$1.26 \cdot 10^9$	61.4	81.8	12.3	$7.2 \cdot 10^{-27}$	$1.6 \cdot 10^{-22}$	11.7	234	7794	0.084	1.7	56
APR $2.0 M_\odot$	$1.39 \cdot 10^9$	60.3	80.4	4.9	$9.7 \cdot 10^{-27}$	$1.8 \cdot 10^{-22}$	14.0	281	9356	0.099	2.0	66
APR $2.21 M_\odot$	$3.15 \cdot 10^8$	84.0	112	1.7	$2.2 \cdot 10^{-26}$	$2.1 \cdot 10^{-22}$	12.7	254	8460	0.094	1.9	62

Table V: Results for the spindown and gravitational wave observables for different neutron stars considered in this work obtained from the semi-analytic expressions eqs. (28), (27), (38), (46), (B3) and (B4). In contrast to the lower mass stars, the $2.21 M_\odot$ neutron star is dense enough to allow for direct Urca reactions. All values are given for a large saturation amplitude $\alpha_{sat} = 1$. The signal to noise ratios are given for the advanced LIGO detector and are obtained with the gravitational wave frequency corresponding to the Kepler frequency as an upper cutoff of the spectrum respectively a fiducial observation interval $\Delta t/t = 10^{-3}$. They are given for sources at three different distances ranging from the Virgo cluster (20 Mpc), and the local group of galaxies (1 Mpc) to a source within the Milky Way (30 kpc).

$$\frac{S}{N} \Big|^{(obs.)} \approx \sqrt{\frac{9\tilde{I}GM R^2}{10D^2} \frac{\Delta\nu}{\bar{\nu} S_h(\bar{\nu})}} = \sqrt{\frac{3GI}{20S_h(\bar{\nu}) D^2} \frac{\Delta t}{t}} \quad (\text{B8})$$

Analogous to the equivalent intrinsic strain eq. (49), this quantity depends on the square of the observation time interval Δt (see also [64]) and depends on the internal composition of the star only via the moment of inertia with uncertainty range eq. (15). Moreover, it depends only on the present (averaged) gravitational wave frequency $\bar{\nu}$ and not the complete spectrum. It is again not directly dependent on the saturation amplitude which only enters indirectly via the dependence on the current frequency via $S_h(\bar{\nu})$. Yet, we stress again that this expression is only valid during the later evolution where the spindown becomes sufficiently slow so that $\Delta\nu \ll \bar{\nu}$. The right part of table V shows the values for the advanced LIGO detector for the different stars and a ratio $\Delta t/t = 10^{-3}$ compared to the previous signal-to-noise estimates. As can be seen in this case the observable signal to noise ratios are more than two orders of magnitude smaller than the total expressions eq. (B5). Nevertheless eq. (B8) still greatly overestimates the detectability since it does not take into account our limited information about the source.

For the advanced LIGO detector the background is nearly constant over the relevant range from 80 to 800 Hz with $S_h^{1/2} \approx 4 \cdot 10^{-24}$ and thereby allows us to further approximate to obtain the simple estimate

$$\frac{S}{N} \Big|_{\text{aLIGO}}^{(obs.)} \approx 50 \sqrt{\frac{\Delta t}{t}} \left(\frac{1 \text{ Mpc}}{D} \right). \quad (\text{B9})$$

Although this expression overestimates the detectability under realistic conditions it might be useful for simple estimates. E.g. for a one year observation period, comparable to past LIGO runs, a source in the Virgo cluster

(20 Mpc) would, in contrast to the early estimates in [47], be impossible to detect unless it is extraordinarily young. A source in our local group of galaxies (1 Mpc) in contrast might be detectable if the results obtained assuming matched filtering do not strongly overestimate the detectability for more realistic search methods. A source in the Milky Way (30 kpc) in contrast could be detectable even if a more realistic search strategy has a significantly lower signal to noise ratio. As discussed before, since the original LIGO detector had a more than an order of magnitude larger background, in contrast to previous estimates [10], it is not surprising that no signal has been detected so far.

Finally let us estimate likely values for the above signal to noise ratios for the examples of possible sources that have been discussed in the main text. As can be seen in table IV, despite the fact that the observable signal-to-noise ratio eq. (B9) is reduced by more than an order of magnitude compared to the total versions eq. (B5), the values are still significantly larger than what one would expect from the detailed analysis in terms of h_0 in the main text. Although the relative sizes for the individual sources are similar, the sensitivity (eq. (49)) which properly takes into account our ignorance of the details of the source leads to systematically lower sensitivities. Correspondingly, one should generally be careful with conclusions based on these alternative sensitivity estimates.

Acknowledgments

We are grateful to Brynmor Haskell, Wynn Ho, Prashant Jaikumar, Feryal Özel and Simin Mahmoodifar for helpful discussions and to the referee for exceptionally constructive advice. This research was supported in part by the Offices of Nuclear Physics and High Energy Physics of the U.S. Department of Energy under contracts #DE-FG02-91ER40628, #DE-FG02-05ER41375.

[1] N. Andersson, *Astrophys. J.* **502**, 708 (1998), gr-qc/9706075.

[2] N. Andersson and K. D. Kokkotas, *Int. J. Mod. Phys.*

- D10**, 381 (2001), gr-qc/0010102.
- [3] M. Alford, S. Mahmoodifar, and K. Schwenzer, *Phys.Rev.* **D85**, 024007 (2012), 1012.4883.
- [4] M. G. Alford, S. Mahmoodifar, and K. Schwenzer, *Phys.Rev.* **D85**, 044051 (2012), 1103.3521.
- [5] N. Andersson, K. D. Kokkotas, and B. F. Schutz, *Astrophys. J.* **510**, 846 (1999), astro-ph/9805225.
- [6] S. L. Shapiro and S. A. Teukolsky, *Black holes, white dwarfs, and neutron stars: The physics of compact objects* (Wiley, 1983).
- [7] C. Palomba, (1999), astro-ph/9912356.
- [8] J. Staff, P. Jaikumar, and R. Ouyed, *Astrophys.J.* **751**, 24 (2012), 1107.1000.
- [9] F. E. Marshall, E. V. Gotthelf, W. Zhang, J. Middleditch, and Q. D. Wang, *Astrophys. J. Lett.* **499**, L179 (1998), arXiv:astro-ph/9803214.
- [10] B. J. Owen *et al.*, *Phys. Rev.* **D58**, 084020 (1998), gr-qc/9804044.
- [11] LIGO Scientific Collaboration, G. M. Harry, *Class.Quant.Grav.* **27**, 084006 (2010).
- [12] N. Andersson *et al.*, *Gen.Rel.Grav.* **43**, 409 (2011), 0912.0384.
- [13] J. Oppenheimer and G. Volkoff, *Phys.Rev.* **55**, 374 (1939).
- [14] R. C. Tolman, *Phys. Rev.* **55**, 364 (1939).
- [15] L. Lindblom, G. Mendell, and B. J. Owen, *Phys. Rev.* **D60**, 064006 (1999), gr-qc/9902052.
- [16] M. G. Alford, S. Mahmoodifar, and K. Schwenzer, *J. Phys.* **G37**, 125202 (2010), 1005.3769.
- [17] M. G. Alford, S. Reddy, and K. Schwenzer, *Phys.Rev.Lett.* **108**, 111102 (2012), 1110.6213.
- [18] B. L. Friman and O. V. Maxwell, *Astrophys. J.* **232**, 541 (1979).
- [19] A. Akmal, V. R. Pandharipande, and D. G. Ravenhall, *Phys. Rev.* **C58**, 1804 (1998), nucl-th/9804027.
- [20] Y. Levin, "Astrophys. J." **517**, 328 (1999), arXiv:astro-ph/9810471.
- [21] W. C. Ho and D. Lai, *Astrophys.J.* **543**, 386 (2000), astro-ph/9912296.
- [22] A. Reisenegger and A. A. Bonacic, (2003), astro-ph/0303454.
- [23] P. Arras *et al.*, *Astrophys. J.* **591**, 1129 (2003), astro-ph/0202345.
- [24] R. Bondarescu, S. A. Teukolsky, and I. Wasserman, *Phys. Rev.* **D79**, 104003 (2009), 0809.3448.
- [25] R. Bondarescu and I. Wasserman, (2013), 1305.2335.
- [26] L. Lindblom, J. E. Tohline, and M. Vallisneri, *Phys. Rev. Lett.* **86**, 1152 (2001), astro-ph/0010653.
- [27] W. Kastaun, *Phys.Rev.* **D84**, 124036 (2011), 1109.4839.
- [28] Y. Wu, C. D. Matzner, and P. Arras, *Astrophys.J.* **549**, 1011 (2001), astro-ph/0006123.
- [29] A. Reisenegger, *Astrophys. J.* **442**, 749 (1995), astro-ph/9410035.
- [30] W. C. Ho, N. Andersson, and B. Haskell, *Phys.Rev.Lett.* **107**, 101101 (2011), 1107.5064.
- [31] B. Haskell, N. Degenaar, and W. C. G. Ho, *Mon. Not. Roy. Astron. Soc.* **424**, 93 (2012), 1201.2101.
- [32] P. S. Shternin and D. G. Yakovlev, *Phys. Rev.* **D78**, 063006 (2008), 0808.2018.
- [33] L. Lindblom, B. J. Owen, and S. M. Morsink, *Phys. Rev. Lett.* **80**, 4843 (1998), gr-qc/9803053.
- [34] P. Jaikumar, G. Rupak, and A. W. Steiner, *Phys. Rev.* **D78**, 123007 (2008), 0806.1005.
- [35] J. Madsen, *Phys. Rev. Lett.* **85**, 10 (2000), astro-ph/9912418.
- [36] N. Andersson, D. I. Jones, and K. D. Kokkotas, *Mon. Not. Roy. Astron. Soc.* **337**, 1224 (2002), astro-ph/0111582.
- [37] B. Haskell, K. Glampedakis, and N. Andersson, (2013), 1307.0985.
- [38] R. N. Manchester, G. B. Hobbs, A. Teoh, and M. Hobbs, *Astron. J.* **129**, 1993 (2005), astro-ph/0412641.
- [39] L. Lindblom and G. Mendell, *Phys.Rev.* **D61**, 104003 (2000), gr-qc/9909084.
- [40] B. Haskell, N. Andersson, and A. Passamonti, (2009), 0902.1149.
- [41] M. G. Alford, S. Mahmoodifar, and K. Schwenzer, (2012), 1209.5962.
- [42] P. Demorest, T. Pennucci, S. Ransom, M. Roberts, and J. Hessels, *Nature* **467**, 1081 (2010), 1010.5788.
- [43] Virgo Collaboration, B. Abbott *et al.*, *Astrophys.J.* **713**, 671 (2010), 0909.3583.
- [44] J. Middleditch, F. E. Marshall, Q. D. Wang, E. V. Gotthelf, and W. Zhang, "Astrophys. J." **652**, 1531 (2006), arXiv:astro-ph/0605007.
- [45] A. G. Lyne, R. S. Pritchard, F. Graham-Smith, and F. Camilo, *Nature* **381**, 497 (1996).
- [46] LIGO Scientific Collaboration, B. Abbott *et al.*, *Astrophys.J.* **683**, L45 (2008), 0805.4758.
- [47] B. J. Owen, *Phys.Rev.* **D82**, 104002 (2010), 1006.1994.
- [48] Q. D. Wang and E. V. Gotthelf, "Astrophys. J." **494**, 623 (1998), arXiv:astro-ph/9708087.
- [49] A. Bonanno, V. Urpin, and G. Belvedere, "Astron.Astrophys.", **451**, 1049 (2006), arXiv:astro-ph/0603034.
- [50] C.-A. Faucher-Giguere and V. M. Kaspi, *Astrophys.J.* **643**, 332 (2006), astro-ph/0512585.
- [51] A. Lyne *et al.*, *Science* **303**, 1153 (2004), astro-ph/0401086.
- [52] K. Thorne, *Rev.Mod.Phys.* **52**, 299 (1980).
- [53] LIGO Collaboration, K. Wette *et al.*, *Class.Quant.Grav.* **25**, 235011 (2008), 0802.3332.
- [54] LIGO Scientific Collaboration, B. Abbott *et al.*, *Phys.Rev.* **D69**, 082004 (2004), gr-qc/0308050.
- [55] LIGO Scientific Collaboration, B. Abbott *et al.*, *Rept.Prog.Phys.* **72**, 076901 (2009), 0711.3041.
- [56] M. Punturo *et al.*, *Class.Quant.Grav.* **27**, 194002 (2010).
- [57] C. O. Heinke and W. C. G. Ho, *Astrophys. J.* **719**, L167 (2010), 1007.4719.
- [58] D. Page, M. Prakash, J. M. Lattimer, and A. W. Steiner, *Phys. Rev. Lett.* **106**, 081101 (2011), 1011.6142.
- [59] D. G. Yakovlev, W. C. G. Ho, P. S. Shternin, C. O. Heinke, and A. Y. Potekhin, *Mon. Not. Roy. Astron. Soc.* **411**, 1977 (2011), 1010.1154.
- [60] J. P. Halpern and E. V. Gotthelf, "Astrophys. J." **709**, 436 (2010), 0911.0093.
- [61] K. S. Long *et al.*, "Astrophys. J." **756**, 18 (2012), 1207.1555.
- [62] LIGO Scientific Collaboration, J. Abadie *et al.*, *Astrophys.J.* **722**, 1504 (2010), 1006.2535.
- [63] L. Lindblom, B. J. Owen, and G. Ushomirsky, *Phys.Rev.* **D62**, 084030 (2000), astro-ph/0006242.
- [64] A. Watts, B. Krishnan, L. Bildsten, and B. F. Schutz, *Mon.Not.Roy.Astron.Soc.* **389**, 839 (2008), 0803.4097.